

RADBOD UNIVERSITY NIJMEGEN

FACULTY OF SCIENCE (FNWI)

HIGH ENERGY PHYSICS

**One-Loop Matching of a Scalar Dark Matter Effective Field
Theory**

Author:

Robin Rietman

Supervisors:

Dr. Susanne Westhoff

Prof. Dr. Wim Beenakker

August 2023



Contents

Introduction	2
1 Theory	4
1.1 Dark Matter	4
1.1.1 Observational Evidence	4
1.1.2 Dark Matter Candidates	6
1.2 Direct Detection	8
1.3 Effective Field Theories	10
1.3.1 Effective Field Theories and their Advantages	11
1.3.2 The Effective Field Lagrangian	11
1.3.3 Fermi's Theory and Matching	13
1.3.4 Dark Matter Effective Field Theories	15
1.4 One-Loop Integrals and Passarino-Veltman Reduction	16
2 Method	19
2.1 The DSMEFT Lagrangian	20
2.2 DSMEFT Feynman Rules	21
2.3 Loop Calculations	25
2.3.1 DSMEFT Loop Amplitude Results	29
2.4 Renormalisation	34
2.5 DLEFT Operators	38
2.6 Matching DSMEFT with DLEFT	39
2.6.1 Tree Level Matching	39
2.6.2 Matching at one-loop Level	40
Conclusion and Discussion	42
Bibliography	43

Introduction

The existence of Dark Matter (DM) is one of the most puzzling challenges that contemporary physics faces. Its existence was proposed due to the observation of unexpected astrophysical behaviour. For example, the rotational velocities of galaxies do not follow the distribution as expected from Newtonian mechanics [1]. From this, one can conclude that we must either adjust Newtonian mechanics, or that we are yet to discover a type of matter than can explain the atypical dynamics. The latter approach leads to the particle interpretation of Dark Matter, which states that DM must be a neutral, non-luminous and weakly interacting particle that is stable, or at least stable on the time scales of the universe. Besides this, the properties of DM are remarkably unconstrained. Many different theories and hypotheses exist, and widely differing masses are proposed.

Although many astrophysical and cosmological observations point us towards the existence of Dark Matter, all this proof remains of indirect nature. The existence of Dark Matter is understood through its effects on gravity, rather than detection of the matter itself. Nowadays, multiple experiments try to probe the nature of DM in a more direct manner. Note that this type of research assumes that DM is also subject to a force other than gravity.

In this thesis, we shall focus on direct detection methods. Direct detection experiments search for recoil signals, induced by DM particles scattering off nuclei or electrons in a detector material. Such scattering signals could allow us to better constrain the mass and cross section of DM particles.

Theoretical physics can aid in this experimental search for DM by predicting what kind of signals may be expected in a detector. Making individual experimental predictions for every DM candidate is quite inefficient, though. This is where the Effective Field Theory (EFT) framework becomes advantageous. EFTs allow one to make a good approximation of a theory that is valid at up to a specific energy scale. The EFT is given by a set of effective interactions, where all higher energy effects are encoded into the coupling constants of the new, lower energy theory. A low energetic effective interaction can be realised by multiple higher energy effects. By searching for DM signals predicted by effective interactions, one can thus probe multiple high energy models at once. In addition, EFTs provide a consistent framework to connect physics at different energy scales, allowing one to relate high-energy DM models to the lower-energy models relevant for direct detection experiments.

This brings us to the subject of this thesis, where we intend to contribute to the research that makes experimental predictions for sub-GeV DM in direct detection experiments. Sub-GeV DM is too light to generate properly measurable nuclear recoil signals, but it can induce electron recoils. At this level, only relatively small energy scales are relevant. The DM particle is of sub-GeV mass, the electron mass is in the MeV range, and the momentum exchange between the DM particle and electron is of sub-MeV order generally. In this scenario, one can use EFTs to separate the high-energy scale, where DM and electron interactions are generated, from the lower-energy scale relevant for direct detection. The relevant low-energy EFT can then be used to make experimental predictions. This makes the application of EFTs a natural fit for electron-scattering direct detection experiments.

We thus propose a Dark Matter EFT with a sub-GeV scalar DM particle. We start from an adapted version of the Standard Model Effective Field Theory, where we add our proposed DM scalar. This is our Dark Standard Model EFT (DSMEFT). Our goal is to match this theory onto a lower energy theory, where all particles with masses above the weak scale are integrated out. Despite the fact that DM EFTs are not new, such matching procedures are almost always performed at leading order, or tree level[2, 3]. The novelty of this research is that we extend the matching procedure to include the next to leading order (NLO) effects. Such NLO effects may provide non-negligible corrections to the leading order matching coefficients, which in turn could influence the experimental predictions one makes. To achieve this, we will calculate all relevant one-loop diagrams in our DSMEFT, which allows us to determine the one-loop matching coefficients. In this study, our interest lies in studying the Wilson coefficients that contribute first at one-loop order. Such NLO coefficients would be quite unconstrained, and this could thus open up interesting possibilities for experimental searches.

Before we move forward to the loop calculations and matching, we shall first discuss some theoretical background in chapter 1. The basics of Dark Matter and Direct Detection will be discussed in respectively sections 1.1 and 1.2. We shall then move to EFTs and their applications in DM research in section 1.3, before finishing with a brief discussion on loop integration in 1.4. In chapter 2 we shall outline our DSMEFT Lagrangian and its corresponding Feynman rules relevant for DM-electron scattering in sections 2.1 and 2.2. After explaining the techniques used to obtain the loop amplitudes in 2.3, we examine the renormalisation needed to obtain finite amplitudes in 2.4. Finally, we discuss the results of matching the proposed DSMEFT to a lower energy theory, DLEFT in section 2.6.

Chapter 1

Theory

1.1 Dark Matter

One of the main questions of fundamental physics nowadays is to understand the nature of so-called Dark Matter. The regular, luminous and baryonic matter that is described by the known laws of physics cannot account for important astrophysical and cosmological observations. Dark Matter is the main proposed entity to explain the occurrences of the above anomalies. In the standard cosmological model, the Λ CDM model, the contribution of regular matter to the matter-energy content of the universe is merely 5%. The vast majority of the matter-energy content of our universe is either Dark Energy or Dark Matter, with the former contributing 69% to the energy budget, and the latter 26%.

More specifically, Dark Matter (DM) contributes to 85% of the matter content of our current universe. In light of the research of this thesis, we shall focus on the topic of Dark Matter. First, we will discuss what specific observations induced the need to include Dark Matter in cosmological models. We shall then take a brief look at possible DM candidates and specify which ones will be relevant for the research done in this thesis.

1.1.1 Observational Evidence

There are many empirical examples that demonstrate the need to include Dark Matter in our physical framework, or, more generally, include a modification of or addition to our current knowledge of the laws of physics. In this section, we shall focus on two of such observational arguments in favour of Dark Matter: the rotational velocities of galaxies and gravitational lensing.

The most well-known example in support of Dark Matter, is the observation of galactic rotational curves. From Newtonian mechanics, one would expect the rotational velocity of stars, dust and gas

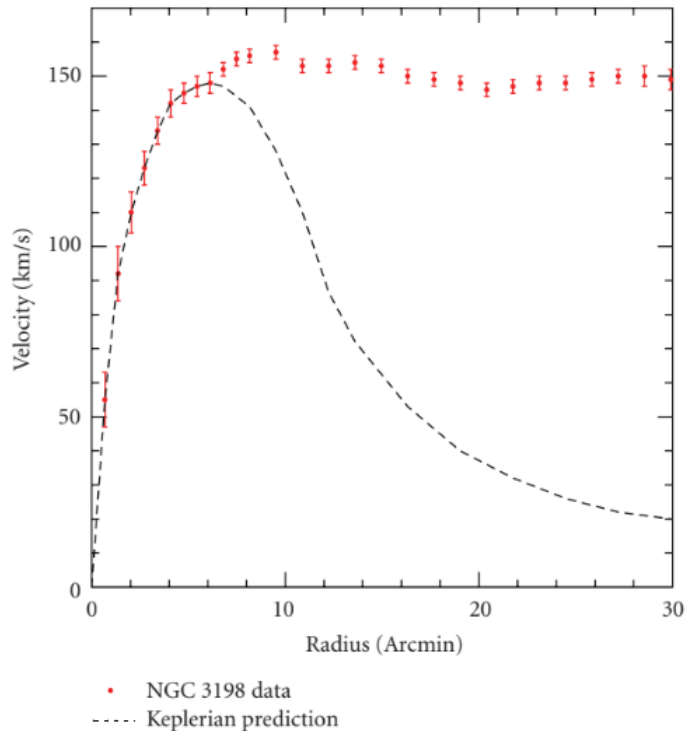


Figure 1.1: Rotational velocities measured in galaxy NCG 3198 compared to the velocities expected by Newtonian mechanics. The velocity is given as a function of the radial distance r to centre of the galaxy. [1]

of galaxies to vary with the radial distance r to the centres of these galaxies with

$$v(r) = \sqrt{\frac{GM(r)}{r}} \quad (1.1)$$

Here, $v(r)$ corresponds to the rotational velocity of the galaxy as a function of r , the radial distance to the centre of the galaxy, whereas $M(r)$ is the mass of the galaxy contained within r . G refers to the Newtonian gravitational constant. At the outskirts of the galaxy, where very little luminous mass is located, we can assume $M(r) \approx M$, with $v(r) \propto r^{-1/2}$ at these regions. This indicates that the expected velocities at the fringe should be lower than velocities closer to the centre of the galaxy. In reality, observations show that the rotational velocities are approximately constant as the distance increases, as illustrated in Figure 1.1.

To account for the fact that $v(r)$ is approximately constant, Newtonian mechanics implies that $M(r) \propto r$. The observations of galaxies do not support such a matter distribution of luminous matter, though. From this deviation of the expected radial velocity, one can infer two possible explanations. Either Newtonian mechanics is incorrect, or unobserved, non-luminous mass could account for the observed dynamics. If one assumes the former position, a modification of Newtonian mechanics called Modified Newtonian Dynamics (MOND) can be used to try to explain the

unexpected observations. The latter position is more mainstream though, and we shall pursue this option. From the proportionality $M(r) \propto r$ we can then deduce that the unobserved matter is clustered in halos extending beyond the peripheries of galaxies. The proposed matter that is missing and non-luminous, is named ‘Dark Matter’. [4].

Another example of observational evidence for the existence of Dark Matter stems from gravitational lensing. This phenomenon originates from the effects of General Relativity (GR). In GR, massive objects influence the curvature of spacetime. By influencing the curvature of spacetime, a massive object will influence the path of other objects in its vicinity as well. Planets orbiting the sun in a elliptical motion are a well-known example of this. The bending of spacetime can affect the path of light as well, and this effect is named ‘gravitational lensing’. The consequences are best observed when observing a galaxy located directly behind another galaxy. In that case, the light emitted by the more distant galaxy appears in the shape of a ring around the galaxy in front. The radius of this ring is the ‘Einstein radius’ θ_E . Through the effect of this lensing, it is possible to determine the mass of the gravitational lens when one knows the Einstein radius [1]:

$$\theta_E = \sqrt{\frac{4GM}{c^2} \frac{d_{LS}}{d_L d_S}} \quad (1.2)$$

G refers to the gravitational constant, c to the speed of light, M to the mass of the lens. d_L, d_S, d_{LS} are the distances respectively to the lens, to the source and from lens to source. Observations of gravitational lensing show that the lensing in many constellations of galaxies is stonger than what can be inferred from the mass of the luminous matter of galaxies. If we again assume that GR is correct, this indicates that galaxies should contain Dark Matter to correctly account for the observed amount of gravitational lensing.[1, 5]

1.1.2 Dark Matter Candidates

We have now identified some examples in favour of Dark Matter. The existence of unexpected dynamics in our universe is strongly established, but the feature that causes these dynamics is still very much unexplained. If we take the Dark Matter avenue, where we assume that Newtonian mechanics and GR are correct, this still leaves us with the important question to understand the nature of such matter. The research in this thesis focuses on detection of particle-like DM. Non-particle candidates do exist, for example in the form of astrophysical objects such as black holes or brown dwarfs. Such candidates are classified as Massive Compact Halo Objects (MACHOs). For brevity, we shall limit ourselves to the discussion of particle-like DM in this section. [1, 6]

Some constraints can be made, but most properties of Dark Matter are unknown. What we do know about DM, is that it is non-luminous. For particle-like DM this means that it does not interact with photons, indicating that DM candidates should be electrically neutral. DM particles should also be stable, or at least very long lived. [7] In addition, observations of the Cosmic Microwave

Background (CMB) also put constraints on the nature of DM. More specifically, CMB data has provided restrictions to the total cosmological baryon density of the universe, which puts constraints on the possibility that DM is of baryonic nature. The current data leads to the conclusion that less than about 20% of the matter content of the universe is of baryonic nature.[8, 9] A proper dark matter candidate is thus of non-baryonic nature. Finally, DM should interact only weakly with regular matter.

The Standard Model contains only one type of particle that agrees with the above mentioned properties: the neutrino. The lightest SM neutrino is stable, massive and weakly interacting. The SM neutrino is not an adequate DM candidate though. Firstly, neutrinos are not abundant enough to account for all DM. Secondly, neutrinos as DM cannot properly account for the large scale structures that are observed in the universe. Neutrinos that to a large extent interact only through gravity, so-called ‘sterile neutrinos’, have been proposed as an alternative neutrino-like DM candidate. Sterile neutrinos with a mass around the keV scale do not run into the same issues as regular neutrinos, making them a possible DM candidate. [9, 10]

We can now conclude that no SM particle can elucidate the nature of dark matter. This indicates that we have to search for new physics beyond the Standard Model (BSM). Nowadays, many models are created with the goal to propose a DM candidate, but it is noteworthy that DM candidates may also be a byproduct of BSM theories. In quite some circumstances BSM theories contain new particles that may be promising DM candidates.

A well-known class of BSM dark matter candidates are the Weakly Interacting Massive Particles (WIMPs). Generally speaking, WIMPs are stable, neutral and weakly interacting particles with a mass in the GeV to TeV range. WIMPs often follow naturally from BSM theories, making them sensible DM candidates. Furthermore, WIMPs with a weak-scale mass naturally produce a relic abundance that agrees with observations. This is the so-called ‘WIMP miracle’ and this seeming coincidence has been a motivation to search for WIMP dark matter.[11] Recent experiments are placing lower and lower upper limits on the DM-nucleon cross section, though. These stringent demands on the DM parameter space have ruled out quite some candidates and models that agree with the WIMP miracle.[12, 13]

Non-WIMP dark matter candidates are also common subjects of inquiry. For example in the form of axions. These particles were originally proposed as a candidate to explain the strong CP problem of Quantum Chromodynamics. Many axion models have masses much smaller than WIMPs, although not necessarily so.[10] The scientific field of DM is certainly wider than the particles that have been discussed here and many more DM candidates have been proposed.

In the remainder of this work, we shall concentrate on WIMP dark matter. The search for WIMPs is an active field of research, with many experimental efforts being made to identify the nature of dark matter. In the next section, we shall delve into the methods that are currently being

used to search for DM.

1.2 Direct Detection

Experiments that aim to measure signals of dark matter particles are a crucial component of the search for dark matter. We have seen that our knowledge of dark matter is based on its gravitational effects. This type of indirect measurement does not always discern between the many different types of DM candidates that have been suggested. Ultimately experimental verification is needed to probe the nature of dark matter. Three main experimental methods exist in the search for DM. Firstly, one can aim to produce it in particle colliders such as the Large Hadron Collider. In this context, DM could appear as a type of missing energy that is not of neutrino origin. Secondly, it is possible to search for the annihilation or decay products of DM candidates. DM is present in astrophysical objects and environments and when propagating through the universe, self annihilation or decay into SM particles could lead to measurable signatures. These methods are referred to as indirect detection. Finally, one can try to detect DM by measuring DM induced atomic recoils.

This latter option is commonly named ‘direct detection’. In the classic conception of direct detection, the goal is to identify nuclear recoils induced by DM - nucleus scattering. An incoming DM particle can scatter off a nucleus and the nucleus will in turn recoil. This recoil signal can be measured, for example by measuring a photon that is emitted. Generally speaking, DM with a mass of about $m_{DM} \approx 10\text{-}10^3$ GeV will lead to a nuclear recoil in the order of 10 keV, although higher and lower recoil energies are possible as well. By identifying which recoil signals point to DM-nucleus scattering, one can determine if a recoil is caused by DM. Direct detection of this type is well suited for WIMPs. These particles have the correct mass range to induce measurable recoils.[14]

The expected rate of WIMPs with mass m_{DM} scattering off a nucleus of mass m_N in a detector with a total target mass of M is given by

$$\frac{dR}{dE_{NR}} = \frac{\rho_0 M}{m_N m_{DM}} \int_{v_{min}}^{v_{esc}} v f(v) \frac{d\sigma}{dE_{NR}} dv \quad (1.3)$$

E_{NR} refers to the nuclear recoil energy, v the DM velocity in the detector’s reference frame and σ stands for the scattering cross section. In addition, ρ_0 and $f(v)$ are astrophysical parameters, respectively the local DM mass density and the normalised DM velocity distribution. Finally, v_{min} is the minimal DM velocity required to induce a nuclear recoil, and v_{esc} is the DM milky way escape velocity.

The DM observables one can extract from this rate are the cross section σ and the DM mass m_{DM} . Direct detection experiments can thus search a mass-cross section parameter space for signals. It is also possible to utilise possible temporal, energetic or directional dependencies to discern the DM signals against background.[15]

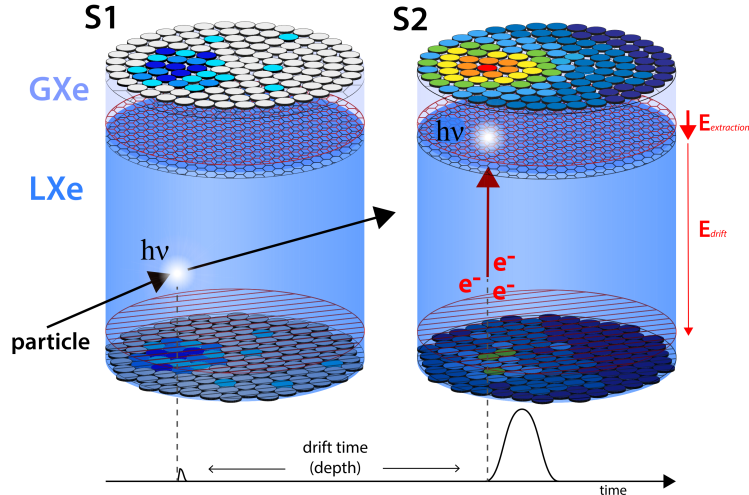


Figure 1.2: Illustration of a dual-phase time projection chamber. On the left hand side, S1, a xenon atom is ionised by an incoming particle. Upon de-excitation, the atom emits a photon that is measured by the photomultiplier tube (PMT) arrays at the top and bottom of the detector. On the right hand side, S2, electrons are produced as a passing particle ionises xenon atoms. If these electrons do not recombine and produce scintillation light, a strong electric field will cause them to drift towards the top PMT array, where the electrons are measured. [18]

The usage of nuclear recoil does pose a disadvantage, due to the fact that DM candidates with sub-GeV mass cannot generate nuclear recoils that are sizable enough to be measured in general. The recoils of bound electrons can be used to study the effects of keV-GeV DM, though. Due to the fact that electrons are of much lower mass, lighter DM candidates can transfer enough momentum to the electron to generate a detectable recoil signal in the range of keV, or smaller. Here one needs to take into account that these electrons are bound in an atomic system, they are thus not on-shell.[16] This requires some extra care when determining the expected detector response, see for example [17].

For this work, it is sufficient to know that we can express both electron and nucleus recoils in terms of the transferred momentum $q = p - k$, where p, k are respectively the outgoing and incoming momenta of the electron or nucleus in center of mass frame. This momentum transfer causes the nucleus to recoil. This recoil can be measured with different detection methods, using either phonons, charge, light or a combination as means of detection.

Liquid noble gas detectors are a common example. In such detectors, the nuclear or electronic targets consist of noble gas atoms. Signals are generated by photons that are released upon de-excitation of nuclei or electrons after a recoil. Modern detectors often combine two measurement methods, though. The XeNON detector is a liquid noble gas dual-phase time projection chamber (TPC), which combines photon detection with charge measurements. An illustration of this type

of detector is given in Figure 1.2. In the latter case, the xenon atoms can be ionised by a passing DM particle. The ionised electrons drift away from the atom as a consequence of a strong electric field that is implemented. If the ionised atoms are not removed from the atom, they will recombine, resulting in an excited xenon atom that will again emit scintillation light.[14]

In this work we will be researching a model with sub-GeV DM mass. As we have seen, such light DM candidates can be researched with direct detection through the measurement of electron recoils. Along with the DM mass, the electron mass and the momentum transfer are relevant parameters. Note that this scenario thus deals with relatively low energy scales. Rather than taking into account all high energy effects, it may be more convenient to use a model that only needs to consider lower energy parameters. Effective Field Theories (EFTs) provide a consistent framework to implement such a model.

1.3 Effective Field Theories

We shall now make the switch from experiment to theory. Direct detection methods provide us with a very precise method to search for dark matter, but theoretical predictions are needed to guide this research. What signals can be expected, what parts of parameter space are of main interest? Particle phenomenology is thus of key importance to bridge the gap between particle dark matter theory and experimentation.

Earlier, we have seen that the nature of DM is still subject to large uncertainties, making it difficult to determine precise definitive guiding principles with regards to mass or cross section. Many particle DM candidates exist within varying mass ranges, which increases the difficulty of research. Focusing on a very specific DM model or candidate seems rather unfruitful in such conditions. Chances are that strict experimental predictions will not cast the net wide enough to detect the rare signals that we are seeking.

This is where the usage of Effective Field Theories (EFTs) in the context of DM may be advantageous. EFTs allow one to make predictions for observables from a theory that is valid at a specific energy range. For direct detection experiments lower energy scales are of main relevance. An EFT can provide a framework to make observation predictions relevant at the energy scale of direct detection. The key idea here is that one does not need to take into account degrees of freedom, or fields, at energies above a certain cutoff scale, greatly increasing the ease of calculation. EFTs additionally have the benefit of being able to probe multiple high energy theories, through the framework of one lower energy theory.

To fully grasp and appreciate the relevance of using Effective Field Theories in DM research, it is vital to discuss the properties of EFTs. Firstly, I shall generally introduce the properties of EFTs and signify the motivation to use such a theory. Then some more technical and mathematical

background will be given. We shall finally discuss how EFTs exactly fit into DM direct detection research. We shall base ourselves on the discussions of [19–21].

1.3.1 Effective Field Theories and their Advantages

Simply put, an Effective Field Theory is a theory that incorporates the relevant fields and degrees of freedom to describe phenomena that are relevant at a specific energy scale. The usage of EFTs makes it possible to make theoretical predictions without the need to know the exact underlying theory. This concept is broadly used in the physical sciences. An architect designing a building needs to incorporate Newtonian mechanics rather than Quantum Electrodynamics (QED). At the energy scale relevant to the architect, other parameters, laws and quantities are relevant.

Newtonian mechanics provides us with successful experimental predictions, but its applicability breaks down at a certain energy scale. In the EFT framework, this upper limit is often referred to as the cutoff scale Λ . At energies $E > \Lambda$ the predictions of the EFT break down, due to the fact that new physics appears which needs to be included in the theoretical framework.

When working with physics at energy scales $E \ll \Lambda$, the advantages of using an EFT are often numerous. Firstly, it allows one to calculate observables without the need for a very detailed theory that explains all short distance, high energy physics. Effects from short scale physics can complicate calculations a lot. In some cases, the knowledge of a shorter scale theory may simply not be present. Leaving out high energy degrees of freedom can thus tremendously increase the ease of calculation, which in turn allows one to focus on the physics that provides a relevant contribution to the calculated observables.

EFTs also provide a method to describe new physics. Operators with dimension $D_M > 4$ can be used to describe the effects of currently unknown small scale physics on lower energy phenomena. Such an effective interaction may be caused by a possible new mediator particle. The EFT itself is agnostic to the exact nature of the possible mediator, though. This allows one to use EFT predictions and measurements at lower energies to seek physics in a bottom-up style. If rare, anomalous events are observed, one can try to extrapolate new, short scale physics from these measurements. [19]. EFTs also provide other benefits, such as the possibility to include nonperturbative effects, but the above mentioned advantages are of special importance to this research.

1.3.2 The Effective Field Lagrangian

An effective field theory is a quantum field theory in itself, with its own dimensional regularisation and renormalisation schemes. Due to this, one can calculate effective Feynman rules and amplitudes without needing to invoke another high energy theory. The fields used in an EFT are also distinct. So, even if an EFT and a more UV complete theory both use a field named ϕ , it does not signify

the same field. The definitions of fields and operators in both theories are linked through a so-called matching procedure. We shall later return to the topics of renormalisation and matching.

To understand the mathematical methodology underlying the EFT approach, one has to understand the EFT Lagrangian \mathcal{L}_{EFT} . A general EFT Lagrangian is expressed as an infinite sum of dimension four local operators \mathcal{O}_i , consisting of light fields. These operators are multiplied by dimensionless Wilson coefficients C_i . This gives the most general expression for our EFT Lagrangian.

$$\mathcal{L}_{EFT} = \sum_i C_i \mathcal{O}_i \quad (1.4)$$

Two things are noteworthy here. Firstly, it is crucial that the EFT incorporates local operators. Locality ensures that a separation of scales can be realised in EFTs. The operators represent the low energy scale, as they only include those fields that are relevant below the threshold Λ . The high energy effects are in turn fully encoded in the Wilson coefficients. The low energy operators are independent from these coefficients and thus independent from effects at high energy.

Secondly, any operator that is admissible by the relevant symmetries of the EFT can be included in this sum. This still leaves one with an infinite sum of operators, vastly too much to be of any practical relevance. This is the reason that EFTs are supplemented with a power counting argument. We define the ratio $\delta = \frac{E}{\Lambda}$, with E being the energy scale one is working with and $E \ll \Lambda$. If the goal is to make predictions with an error at δ^{n+1} order of magnitude, the Lagrangian needs to be expanded up to δ^n . This accuracy can be reached with a finite amount of terms in the Lagrangian. In this manner an EFT can be adjusted to be more or less accurate, depending on the application. The parameters in the EFT Lagrangian can then be determined by performing a set of measurements at the relevant energy scale.

If we apply this power counting argument to \mathcal{L}_{EFT} , we can interpret our Lagrangian as an expansion over $\frac{1}{\Lambda}$ [19]:

$$\mathcal{L}_{EFT} = \mathcal{L}_4 + \sum_{D_M > 4} \frac{\mathcal{L}_{D_M}}{\Lambda^{D_M-4}} \quad (1.5)$$

$$= \mathcal{L}_4 + \sum_{D_M > 4} \frac{C_i^{D_M-4} \mathcal{O}_i^{D_M-4}}{\Lambda^{D_M-4}} \quad (1.6)$$

$$= \mathcal{L}_4 + \frac{\mathcal{L}_5}{\Lambda} + \frac{\mathcal{L}_6}{\Lambda^2} + \mathcal{O}\left(\frac{1}{\Lambda^3}\right) \quad (1.7)$$

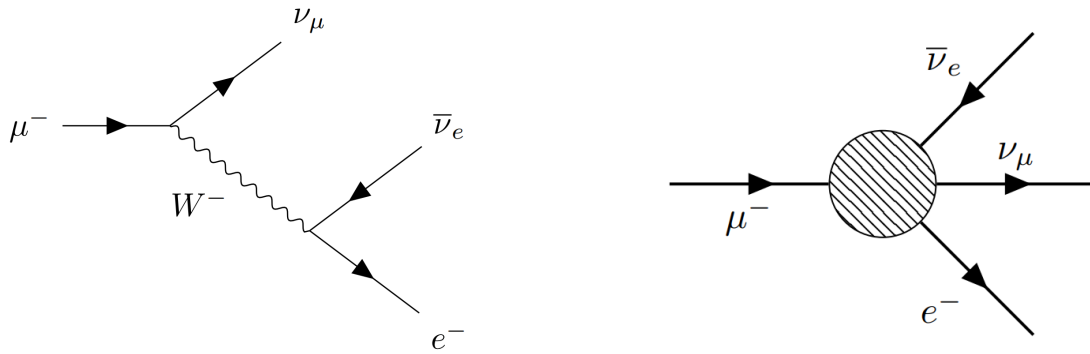
The EFT Lagrangian can thus be organised as a sum of operators with increasing mass dimensions D_M , divided by the high energy cutoff scale Λ . An EFT can thus include operators higher than dimension 4, a feature that does not occur in regular, renormalisable quantum field theories.¹ The operators with $D_M > 4$ can be interpreted as corrections of the order $\delta = \frac{E}{\Lambda}$ in observables. Operators

¹The occurrence of operators with $D_M > 4$ does not mean that EFTs are fundamentally unrenormalisable. A diagram including two insertions of a \mathcal{L}_5 term can be renormalised by a \mathcal{L}_6 term, and so on.

with higher dimensions are thus suppressed by a factor of δ^{D_M-4} . Higher dimensional operators are nevertheless still of interest in EFTs. On the one hand due to the fact that they increase the accuracy of the EFT's predictions, which is especially relevant when performing high precision experiments. On the other hand, higher dimensional operators can inform us about new physics that may occur above the cutoff scale, unless lower dimensional operators have already described the effects of new physics. We shall illustrate this last point, as well as the relevance of EFTs in general, by means of an example.

1.3.3 Fermi's Theory and Matching

The most often used example of an EFT is probably Fermi's theory. Its success stems from the fact that this theory allowed physicists to perform calculations involving weak decays even before the W and Z boson were known. Let us look at the decay of the muon for an example. Figure 1.3a shows the Feynman diagrams corresponding to the decay of the muon in terms of the Standard Model, whereas Figure 1.3b describes the decay in terms of the effective Fermi theory. Note that the latter is a four fermion interaction, with $D_M = 6$. Using (1.7), we instantly recognise that the effective coupling must have a mass dimension of -2, originating from the factor Λ^{-2} . This effective coupling is historically named G_F .



(a) Decay of a muon in the full theory, including the W boson mediator

(b) Decay of a muon as an effective, four fermion interaction in Fermi's theory

Figure 1.3: The decay of a muon.

Both the Standard Model and Fermi's theory should produce the same amplitude, as they are different methods to calculate the same object. This is due to the fact that the muon mass is much smaller than the W boson mass, as we will see. To ensure that both theories agree, one has to perform a so-called matching procedure. Matching relates the couplings of the EFT to those of the

higher energy theory. The Fermi Lagrangian for the effective interaction is written as

$$\mathcal{L}_{Fermi} = -\frac{4G_F}{\sqrt{2}}(\bar{e}\gamma_\rho P_L\nu_e)(\bar{\nu}_\mu\gamma^\rho P_L\mu) \quad (1.8)$$

with e, μ, ν_μ and ν_e denoting the electron, muon and neutrino fields, and $P_L = \frac{1}{2}(1 - \gamma^5)$ being the left-handed projection operator. We thus have to relate the coefficient $\frac{4G_F}{\sqrt{2}}$ to the amplitude of the Standard Model description of muon decay. This amplitude is

$$\mathcal{A}_{SM} = -\frac{g^2}{2}(\bar{u}_e\gamma_\rho P_L v_{\nu_e})\frac{-ig^{\rho\sigma}}{p^2 - M_W^2}(\bar{u}_{\nu_\mu}\gamma_\sigma P_L u_\mu) \quad (1.9)$$

with the electroweak $SU(2)_W$ coupling constant g , and the spinors u_μ, u_e, v_{ν_e} and u_{ν_μ} . We now use the fact that we are in a regime where all momenta are much smaller than M_W , so that $p^2/M_W^2 \ll 1$. This allows us to expand the propagator of the W boson

$$\frac{1}{p^2 - M_W^2} = -\frac{1}{M_W^2}\left(1 + \frac{p^2}{m_W^2} + \dots\right) \quad (1.10)$$

$$\approx -\frac{1}{M_W^2} \quad (1.11)$$

The propagator can thus be approximated to be constant in the energy regime relevant for Fermi's theory. If we plug (1.11) back into the amplitude of (1.9), we find

$$\mathcal{A}_{SM} = -i\frac{g^2}{2M_W^2}(\bar{u}_e\gamma_\rho P_L v_{\nu_e})(\bar{u}_{\nu_\mu}\gamma_\rho P_L u_\mu) \quad (1.12)$$

This amplitude originates from the local Lagrangian

$$\mathcal{L} = -\frac{g^2}{2M_W^2}(\bar{e}\gamma_\rho P_L\nu_e)(\bar{\nu}_\mu\gamma^\rho P_L\mu) \quad (1.13)$$

Combining (1.8) with (1.13) allows us to relate the coefficients of both Lagrangians to one another

$$\frac{G_F}{\sqrt{2}} = \frac{g^2}{8M_W^2} \quad (1.14)$$

The value of G_F can be established by performing measurements on the muon lifetime and one can then use Fermi's theory to make parameter-free predictions for decay distributions of the muon. We also recognize that the expansion made in (1.11) breaks down once $p \approx M_W$. At this scale, the effects of the W boson propagator cannot be ignored anymore.

Fermi's constant also has predicted the range where new physics should appear, causing the EFT to break down. We can relate G_F to the vacuum expectation value $v = \frac{2M_W}{g}$, obtaining

$$\frac{G_F}{\sqrt{2}} = \frac{1}{2v^2} \quad (1.15)$$

$$(\sqrt{2}G_F)^{-1/2} = v \quad (1.16)$$

$$= 246 \text{ GeV} \quad (1.17)$$

Higher dimensional effective operators can thus indicate where new physics may appear. In the case of Fermi's theory, the determination of G_F allowed one to predict at what scale possible new physics may arise. This promise was fulfilled when the W and Z boson were later identified to have masses of respectively about 80 and 91 GeV.

1.3.4 Dark Matter Effective Field Theories

Now that we have finished our general discussion of Effective Field Theories, we switch to the application of EFTs in dark matter research, which is becoming more and more prevalent. We shall focus our discussion on the usage of EFTs in direct detection searches for DM.

Remember that direct detection experiments work at typical energy scales in the MeV range for DM and nucleus/electron momentum transfer, giving recoils in the keV range. These relatively low energies make direct detection experiments a natural candidate to invoke the use of EFTs. One can ignore heavy particles, such as the W^\pm , Z and Higgs bosons by including their effects in the Wilson Coefficients. The electron mass and momentum are of the same order of magnitude in this experimental context, and they can explicitly not be ignored when working with an EFT at lower energies.

The applications of EFTs can increase the ease of calculations, as one does not need the more complicated higher energy theory to make experimental predictions. By proposing a type of particle and its properties, the relevant symmetries and the energy range, an effective DM Lagrangian can be constructed. This Lagrangian can then be used to model the interactions between DM and SM particles, without the need to invoke a more UV complete theory.

In addition to this, EFTs also offer the possibility to search for DM in a more model independent manner. DM experiments are often model driven. A theory with a specific DM candidate can be used to make experimental predictions. The obvious downside is that such searches are quite narrow, a large inconvenience when searching for something as unknown as DM. EFTs meanwhile only describe an effective interaction between DM and SM particles at a lower energy. The idea is that an effective interaction can be realised by multiple mediators or types of interactions at higher energies. The EFT itself is agnostic to such interactions, though, and it can probe the effective interactions without the need to know the higher energy theory. One can then work either top-down, by deriving an EFT that probes multiple types of mediators simultaneously, or bottom-up, by searching for anomalous signals.

The research field of DM EFTs is very lively. On the theory side, predictions for direct detection experiments are made by taking a high energy model and deriving the relevant EFTs [3, 22, 23]. Well known direct detection experiments, such as XENON, are also performing nuclear recoil experiments to study different DM EFTs [24].

An idea that is often invoked in DM EFT research is the Higgs portal. As we have seen, DM should only be weakly interacting with SM particles. The Higgs boson could perhaps be a mediator between DM and SM particles. In other words: the Higgs boson could be the ‘portal’ between the DM and SM sectors. EFTs relevant for direct detection work well below the mass scale of m_H . One could thus reduce the tree level diagram with a Higgs boson mediating the SM-DM interaction to an effective SM-DM interaction. A general example is given in Figure 1.4. Such simple Higgs

portal models are becoming more and more constrained though [25]. The increasing precision of direct detection has thus ruled out the most simple Higgs portal models, in addition to ruling out the simplest WIMP models. This signifies the need for more advanced DM-SM interactions, for example at one-loop level. DM EFTs that include one-loop corrections have not been studied extensively yet, and they could open a new type of portal to DM. To study the effect of loop corrections on EFTs, one needs to implement less than trivial loop calculations. We shall now shift our discussion to a method that allows us to perform loop calculations.

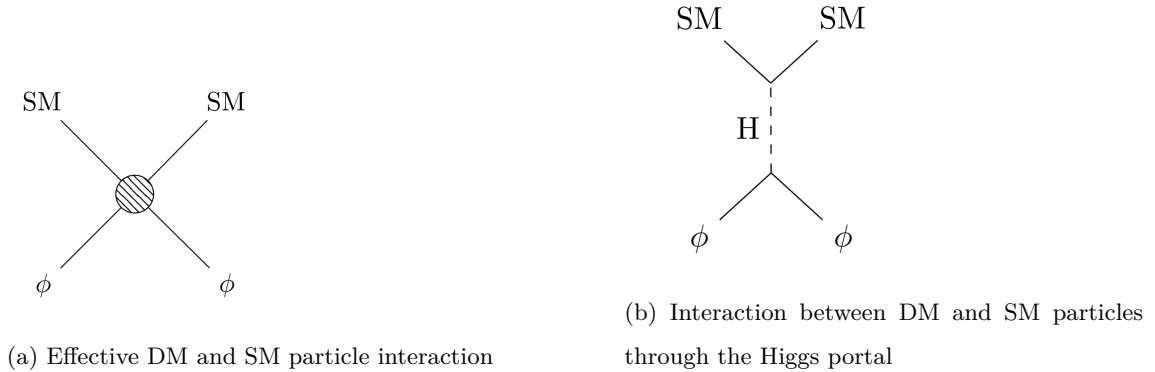


Figure 1.4: A general sketch of the interaction between Standard Model particles SM and a generic DM particle ϕ .

1.4 One-Loop Integrals and Passarino-Veltman Reduction

We have seen how EFT's and Direct Detection experiments allow us to search for signals of dark matter. As experimental precision has increased, some DM hypotheses have been ruled out. This development signifies the need for new theoretical predictions. It also points towards direct detection experiments becoming more and more precise, though.

In order to properly cater to these developments, one needs to include the effects of next to leading order (NLO) diagrams when working with DM EFTs. To achieve this, one needs to comprehensively research what DM and SM interactions emerge at one-loop level. This study aims to contribute to that goal. One-loop calculations are an important aspect in the search for better theoretical predictions. Such calculations are not trivial and multiple methods have been developed to properly assess them.

One of those methods is Passarino-Veltman reduction, which reduces a one-loop tensor integral to scalar integrals[26, 27]. Despite the fact that Passarino-Veltman reduction has its limitations [28], it is still widely used and very useful due to its well-defined procedure. In this work we shall later on implement Passarino-Veltman reduction to calculate one-loop DM-electron scattering diagrams.

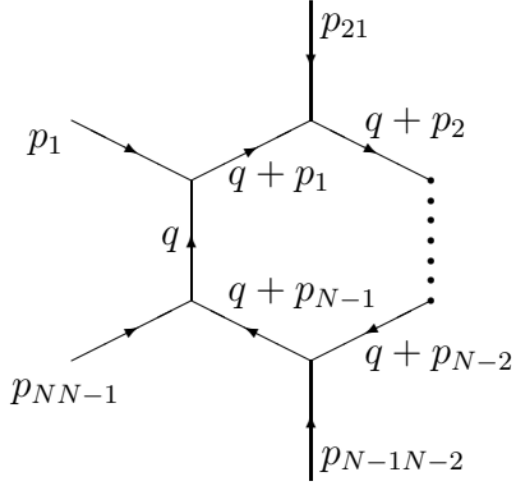


Figure 1.5: Conventions for the N point loop integral, where p_{21} refers to the notation $p_{21} = p_2 - p_1$, and q is the loop momentum.[29]

To grasp this method, let us first give a general definition of a one-loop integral in D spacetime dimensions with N propagator factors in the denominator and loop momentum l . Here, p_1 to p_{N-1} denote the independent external momenta and μ_1 to μ_P refer to the open Lorentz indices of the tensor integral [29]. In addition we introduce μ , a parameter with mass dimension that is meant to fix the mass dimension of the integral when varying the spacetime dimensionality D. These conventions are also summarised in Figure 1.5.

$$T_{\mu_1 \dots \mu_P}^N(p_1, \dots, p_{N-1}, m_0, \dots, m_{N-1}) = \frac{(2\pi\mu)^{4-D}}{i\pi^2} \int d^D l \frac{l_{\mu_1} \dots l_{\mu_P}}{D_0 D_1 \dots D_{N-1}} \quad (1.18)$$

$$D_0 = l^2 - m_0^2 + i\epsilon \quad (1.19)$$

$$D_i = (l + \sum_{k=1}^i p_k)^2 - m_i^2 + i\epsilon \quad (1.20)$$

The goal is to reduce (1.18) to a set of known scalar integrals. A four-point tensor integral for example can ultimately be reduced to the scalar integrals that involve one, two, three or four propagator factors in the denominator. In the application of our scalar DM EFT, we only need the first three, which are defined as follows

$$A_0(m^2) = \frac{(2\pi\mu)^{4-D}}{i\pi^2} \int d^D l \frac{1}{(l+p)^2 - m^2} \quad (1.21)$$

$$B_0(p^2, m_1^2, m_2^2) = \frac{(2\pi\mu)^{4-D}}{i\pi^2} \int d^D l \frac{1}{(l^2 - m_1^2)((l+p)^2 - m_2^2)} \quad (1.22)$$

$$C_0(p_1^2, p_2^2, (p_1 + p_2)^2, m_1^2, m_2^2, m_3^2) = \frac{(2\pi\mu)^{4-D}}{i\pi^2} \int d^D l \frac{1}{(l^2 - m_1^2)((l+p_1)^2 - m_2^2)((l+p_1+p_2)^2 - m_3^2)} \quad (1.23)$$

The analytical results of these scalar integrals are known, which allows us to find the full result of the one-loop tensor integral after Passarino-Veltman reduction. We shall illustrate the reduction of a tensor integral to scalar Passarino-Veltman integrals by means of a simple example. Let us take a look at a two-point function with open Lorentz index μ and masses of the loop particles m_1 and m_2 :

$$B_\mu = \frac{(2\pi\mu)^{4-D}}{i\pi^2} \int d^D l \frac{l_\mu}{(l^2 - m_1^2)((l+p)^2 - m_2^2)} \quad (1.24)$$

The Lorentz decomposition of this term is given by

$$B_\mu = B_1(p^2, m_1^2, m_2^2)p_\mu \quad (1.25)$$

and we note that p_μ is the only momentum four-vector, and p^2, m_1^2 and m_2^2 are the only scalar invariants that the integral can produce after integrating over l . The scalar tensor coefficient B_1 can be determined by projecting onto p_μ and using the fact that $(l+p)^2 = p^2 + l^2 + 2l \cdot p + (m_1^2 + m_2^2) - (m_1^2 + m_2^2)$.

$$p^\mu B_\mu = B_1(p^2, m_1^2, m_2^2)p^2 \quad (1.26)$$

$$= \frac{(2\pi\mu)^{4-D}}{i\pi^2} \int d^D l \frac{l \cdot p}{(l^2 - m_1^2)((l+p)^2 - m_2^2)} \quad (1.27)$$

$$= \frac{(2\pi\mu)^{4-D}}{i\pi^2} \int \frac{d^D l}{2} \frac{(l+p)^2 - m_2^2 - (l^2 - m_1^2) - (p^2 + m_1^2 - m_2^2)}{(l^2 - m_1^2)((l+p)^2 - m_2^2)} \quad (1.28)$$

$$= \frac{(2\pi\mu)^{4-D}}{i\pi^2} \int \frac{d^D l}{2} \left[\frac{1}{l^2 - m_1^2} - \frac{1}{(l+p)^2 - m_2^2} - \frac{p^2 + m_1^2 - m_2^2}{(l^2 - m_1^2)((l+p)^2 - m_2^2)} \right] \quad (1.29)$$

where we have used $l \cdot p = \frac{1}{2}[(l+p)^2 - m_2^2 - (l^2 - m_1^2) - (p^2 + m_1^2 - m_2^2)]$ to rewrite the integral. We recognize the scalar integrals $A_0(m_1^2)$, $A_0(m_2^2)$ and $B_0(p^2, m_1^2, m_2^2)$ when combining (1.29) with (1.21) and (1.22)

$$B_1(p^2, m_1^2, m_2^2) = \frac{1}{2p^2} \left[A_0(m_1^2) - A_0(m_2^2) - (p^2 + m_1^2 - m_2^2)B_0(p^2, m_1^2, m_2^2) \right] \quad (1.30)$$

This example illustrates how one can calculate a loop integral by reducing it to a combination of scalar integrals, where the Passarino-Veltman scalar integrals are the coefficients of the decomposed tensor integral. Most realistic loop calculations are much more difficult to work out by hand, stressing the need for automation of the procedure. For example, when the numerator of a loop integral contains two loop momenta that each carry a Lorentz index, $l_\mu l_\nu$, one must project onto the metric tensor $g_{\mu\nu}$ in addition to projecting onto all symmetric tensors $p_\mu q_\nu$ that are constructed from the independent external momenta featuring in the loop integral.

Nowadays Passarino-Veltman reduction is performed by software packages, such as the Mathematica package FeynCalc [30]. The explicit expressions of the scalar integrals can be found with additional packages [31, 32]. In this work we shall extensively make use of Passarino-Veltman reduction by means of these packages to perform one-loop calculations.

Chapter 2

Method

In the previous chapter we have discussed how the framework of Effective Field Theories can be of use in the search for dark matter, especially in direct detection experiments. In the area of DM EFTs, we noted that the simplest Higgs portal models have been strongly constrained already. This signifies the need for two things. Firstly, the addition of loop effects to the tree level Higgs portal may provide new, unexplored channels in the search for DM. So, even if the DM-SM interaction through the Higgs portal is strongly constrained, this does not yet properly inform us about the relevance of DM-SM interactions at one-loop order, highlighting the need to include loop calculations when researching DM-SM interactions.

Secondly, DM EFTs should include operators with $D_M > 4$ as these higher dimensional operators can generate additional corrections. The addition of next to leading order effects remains a relatively unexplored field though. Current DM EFTs are mainly matched on tree level, leaving out the possible effects that next to leading order effects may have on the relations between the respective high and low energy couplings. In this work, we aim to perform exactly such a matching at one-loop level for a DM EFT. The focus will be on electron-DM scattering in noble gas direct detection experiments, such as XENON.

To achieve this, several steps must be taken. We shall commence by specifying the definition of our high energy DM EFT Lagrangian, which is used to determine all Feynman rules relevant for electron-DM scattering. Then we discuss the computation of the loop diagram amplitudes, and the techniques and relations that were used. Thereafter the renormalisation procedure of our DM EFT shall be outlined, which is needed to obtain non-divergent amplitudes. Finally, we identify the low energy DM EFT Lagrangian, allowing us to determine the one-loop matching between the high and low energy DM EFTs.

2.1 The DSMEFT Lagrangian

Let us start by defining the general form of our effective dark matter Lagrangian. This Lagrangian is defined by a cutoff scale of $\Lambda_{EW} = v$, with v being the SM vacuum expectation value of approximately 246 GeV. The Lagrangian thus contains all SM particles and interactions, and it is supplemented by DM scalars, denoted with ϕ . We shall refer to this Lagrangian as the DSMEFT Lagrangian.

Our proposed DM particle ϕ is a stable singlet under SM symmetries with spin 0. We additionally implement that ϕ is odd under a \mathbb{Z}_2 symmetry, whereas all SM particles are even. This symmetry guarantees that our DM scalar is stable. Our DM scalar is of sub GeV mass, which is the mass range where electron-DM scattering is relevant, as we have seen in section 1.2.

The DSMEFT Lagrangian consists of all SM interactions, with additional dimension 6 SM-DM interactions. The operators written here are given by [2], and only operators including solely scalar DM particles are selected. Dimension 5 operators are omitted, as our goal is to match onto the $ee\phi\phi$ effective scattering interaction at lower energies. This requires our interactions to contain operators with two scalar DM insertions, which are only realised by the dimension 6 operators given in [2]. We then obtain the DSMEFT Lagrangian given by (2.1), where we use a summation convention for I, a, i such that $W_{\mu\nu}^I W^{I,\mu\nu}$ refers to $\sum_I W_{\mu\nu}^I W^{I,\mu\nu}$, and so on.

$$\begin{aligned}
\mathcal{L}_{DSMEFT} = & \frac{C_{H^4\phi^2}}{\Lambda^2} (H^\dagger H)^2 \phi^2 + \frac{C_{H^2\phi^4}}{\Lambda^2} (H^\dagger H) \phi^4 + \frac{C_{B\phi^2}}{\Lambda^2} B_{\mu\nu} B^{\mu\nu} \phi^2 \\
& + \frac{C_{W\phi^2}}{\Lambda^2} W_{\mu\nu}^I W^{I,\mu\nu} \phi^2 + \frac{C_{G\phi^2}}{\Lambda^2} G_{\mu\nu}^a G^{a,\mu\nu} \phi^2 \\
& + \frac{C_{\tilde{B}\phi^2}}{\Lambda^2} \tilde{B}_{\mu\nu} B^{\mu\nu} \phi^2 + \frac{C_{\tilde{W}\phi^2}}{\Lambda^2} \tilde{W}_{\mu\nu}^I W^{I,\mu\nu} \phi^2 \\
& + \frac{C_{\tilde{G}\phi^2}}{\Lambda^2} \tilde{G}_{\mu\nu}^a G^{a,\mu\nu} \phi^2 + \frac{C_{(DH)^2\phi^2}}{\Lambda^2} (D_\mu H)^\dagger (D^\mu H) \phi^2 \\
& + Y_d^{ii} \frac{C_{d\phi^2}}{\Lambda^2} (\bar{Q}_L^i H d_R^i) \phi^2 + h.c. + Y_u^{ii} \frac{C_{u\phi^2}}{\Lambda^2} (\bar{Q}_L^i \tilde{H} u_R^i) \phi^2 + h.c. \\
& + Y_e^{ii} \frac{C_{e\phi^2}}{\Lambda^2} (\bar{L}_L^i H e_R^i) \phi^2 + h.c. + \mathcal{L}_{SM}
\end{aligned} \tag{2.1}$$

In this Lagrangian, H refers to the Higgs doublet, and $B_{\mu\nu}, W_{\mu\nu}^I, G_{\mu\nu}^a$ are the gauge field tensors, with $\tilde{B}_{\mu\nu}, \tilde{W}_{\mu\nu}^I, \tilde{G}_{\mu\nu}^a$ being the corresponding dual tensors. Q_L^i and L_L^i are the left handed quark and lepton doublet with generation label i , whereas d_R^i, u_R^i and e_R^i are the right handed down and up quark and lepton singlets. Note that we use mass eigenstates for all the fermions. Finally, D_μ is the covariant derivative that pertains to the Higgs doublet. Exact definitions are given below in 2.2. Here we have defined the Yukawa couplings $Y_f = \sqrt{2} \frac{m_f}{v}$ as a diagonal matrix with index ii . By this definition, no additional mixing between fermion generations occurs at tree level.

2.2 DSMEFT Feynman Rules

It is now possible to directly determine the DSMEFT Feynman rules based on (2.1). As our goal is to apply the DSMEFT to electron scattering in direct detection, we stress two points. Firstly, all DM scalars ϕ are identical. Secondly, we are interested in those Feynman rules that are relevant for the one-loop $ee\phi\phi$ scattering amplitudes. All operators that include gluons and quarks can be left out, for example, as these will only contribute at two loop level or higher. There is one exception: the top quark can contribute at one-loop order. Due to time constraints, the calculation of one-loop top quark contributions was excluded. ¹We adopt the following conventions, consistent with [29].

Firstly, we use the following definition of the gauge fields:

$$B_{\mu\nu} = \partial_\mu B_\nu - \partial_\nu B_\mu \quad (2.2)$$

$$W_{\mu\nu}^I = \partial_\mu W_\nu^I - \partial_\nu W_\mu^I + g\epsilon^{IKL}W_\mu^K W_\nu^L \quad (2.3)$$

$$G_{\mu\nu}^a = \partial_\mu G_\nu^a - \partial_\nu G_\mu^a + g_s f^{abc}G_\mu^b G_\nu^c \quad (2.4)$$

with indices $a = 1, \dots, 8$ and $I = 1, 2, 3$. The dual field strength tensors are given by $\tilde{B}_{\mu\nu} = \frac{1}{2}\epsilon_{\mu\nu\alpha\beta}B^{\alpha\beta}$, and so on.

The covariant derivative corresponds to:

$$D_\mu = \partial_\mu - igI_W^I W_\mu^I + ig'\frac{Y_W}{2}B_\mu - i\frac{g_s}{2}\lambda_a G_\mu^a \quad (2.5)$$

Applied to the Higgs doublet, this covariant derivative takes the following shape, using $Y_W = 1$ for the Higgs doublet:

$$D_\mu = \partial_\mu - igI_W^I W_\mu^I + i\frac{g'}{2}B_\mu \quad (2.6)$$

I_W^I refers to the weak isospin generator $I_W^I = \frac{\sigma^I}{2}$, Y_W to weak hypercharge and λ_a to the Gell-Mann matrices. This is the most general definition of the covariant derivative, but note that depending on the field that D_μ is applied to, only part of it may be of relevance

The gauge eigenstates and physical mass eigenstates of electroweak bosons are related by:

$$W_\mu^\pm = \frac{1}{\sqrt{2}}(W_\mu^1 \mp iW_\mu^2) \quad (2.7)$$

$$\begin{pmatrix} Z_\mu \\ A_\mu \end{pmatrix} = \begin{pmatrix} \cos(\theta_W) & \sin(\theta_W) \\ -\sin(\theta_W) & \cos(\theta_W) \end{pmatrix} \begin{pmatrix} W_\mu^3 \\ B_\mu \end{pmatrix} \quad (2.8)$$

$$(2.9)$$

¹The quark one-loop diagrams that are possible, are suppressed by a factor of m_f/v . Thus only the one-loop diagram containing two top quarks can be relevant.

The mass eigenstates on the left hand side correspond to the physical bosons, the W^\pm, Z and γ . Here, θ_W refers to the Weinberg or weak mixing angle, which can be expressed in the $SU(2)_L$ and $U(1)_Y$ couplings, respectively g and g' :

$$\cos(\theta_W) = \frac{g}{\sqrt{g^2 + g'^2}} \quad (2.10)$$

$$\sin(\theta_W) = \frac{g'}{\sqrt{g^2 + g'^2}} \quad (2.11)$$

$$(2.12)$$

One can relate the electrical charge $e = \sqrt{4\pi\alpha}$ to these couplings and mixing angles by $g = e/\sin(\theta_W)$.

The fermion fields occurring in the Lagrangian refer to physical mass eigenstate left handed quark doublets Q_L^i and lepton doublets L_L^i with generation label i :

$$Q_L^i = \begin{pmatrix} u_L^i \\ d_L^i \end{pmatrix} \quad (2.13)$$

$$L_L^i = \begin{pmatrix} \nu_L^i \\ e_L^i \end{pmatrix} \quad (2.14)$$

d_R^i, u_R^i and e_R^i in turn denote right handed physical mass eigenstate singlets .

We implement 't Hooft-Feynman gauge when working with the Higgs field. The Higgs doublet and its conjugate are given by:

$$H = \begin{pmatrix} G_+ \\ \frac{v+h+iG_0}{\sqrt{2}} \end{pmatrix} \quad (2.15)$$

$$\tilde{H} = \begin{pmatrix} \frac{v+h-iG_0}{\sqrt{2}} \\ -G_- \end{pmatrix} \quad (2.16)$$

where G_\pm, G_0, h all correspond to fields, with the former two being the Goldstone boson fields and h the physical Higgs boson field. Additionally, $v = \frac{2m_W}{g} \approx 246$ GeV is the vacuum expectation value.

When implementing 't Hooft-Feynman gauge, the Z and W boson propagators are given by:

$$W_\mu \xrightarrow{p} W_\nu = \frac{-ig_{\mu\nu}}{p^2 - m_W^2} \quad (2.17)$$

$$Z_\mu \xrightarrow{p} Z_\nu = \frac{-ig_{\mu\nu}}{p^2 - m_Z^2} \quad (2.18)$$

For $G = G_0, G_+, G_-$, the Goldstone boson propagator is given by

$$G \xrightarrow{p} G = \frac{i}{p^2 - m_G^2} \quad (2.19)$$

Finally, the masses of the W and Z boson are $m_W = \frac{1}{2}vg$ and $m_Z = \frac{1}{2}v\sqrt{g^2 + g'^2}$, and the photon A is massless. The Goldstone boson masses are given by $m_{G_0} = m_Z$ and $m_{G_{+/-}} = m_W$

By convention, we multiply the vertices originating from the Lagrangian by i to obtain the final Feynman rules for the DSMEFT vertices. Two approaches have been taken to verify the Feynman rules. Firstly, the Feynman rules were calculated manually. Afterwards the calculation was automatized by the usage of FeynRules [33]. We then obtain the following Feynman Rules.

$$\begin{aligned}
 & \text{Diagram (2.20): } Z_\nu \text{ (wavy), } H \text{ (dashed) } \rightarrow Z_\mu \text{ (wavy), } \phi \text{ (dashed), } \phi \text{ (dashed)} \\
 & = 2ig_{\mu\nu} \frac{C_{(DH)^2\phi^2}}{\Lambda^2} \frac{mzg}{\cos(\theta_W)} \quad (2.20) \\
 & \text{Diagram (2.22): } W_\nu^- \text{ (wavy), } H \text{ (dashed) } \rightarrow W_\mu^+ \text{ (wavy), } \phi \text{ (dashed), } \phi \text{ (dashed)} \\
 & = 2ig_{\mu\nu} \frac{C_{(DH)^2\phi^2}}{\Lambda^2} m_W g \quad (2.22)
 \end{aligned}$$

$$\begin{aligned}
 & \text{Diagram (2.21): } \phi \text{ (dashed), } e \text{ (solid)} \rightarrow \phi \text{ (dashed), } e \text{ (solid)} \\
 & = 2i \frac{C_{e\phi^2}}{\Lambda^2} m_e \quad (2.21) \\
 & \text{Diagram (2.23): } H \text{ (dashed), } \phi \text{ (dashed)} \rightarrow \phi \text{ (dashed)} \\
 & = 2i \frac{C_{H^4\phi^2}}{\Lambda^2} \left(\frac{2m_W}{g} \right)^3 \quad (2.23)
 \end{aligned}$$

$$\begin{aligned}
& \text{Diagram 1: } W_\mu^+ \text{ and } W_\nu^- \text{ meet at a vertex with incoming momenta } p \text{ and } q, \text{ and outgoing } \phi \text{ bosons.} \\
& = -8i \frac{C_{W\phi^2}}{\Lambda^2} (g_{\mu\nu} p \cdot q - p_\nu q_\mu) \\
& \quad + 2i \frac{C_{(DH)^2\phi^2}}{\Lambda^2} g_{\mu\nu} m_W^2 \\
& \text{Diagram 2: } G_+ \text{ and } G_- \text{ meet at a vertex with incoming momenta } p \text{ and } q, \text{ and outgoing } \phi \text{ bosons.} \\
& = 2i \frac{C_{H^4\phi^2}}{\Lambda^2} \left(\frac{2m_W}{g} \right)^2 \\
& \quad - 2i \frac{C_{(DH)^2\phi^2}}{\Lambda^2} p \cdot q
\end{aligned} \tag{2.24}$$

$$\begin{aligned}
& \text{Diagram 1: } Z_\mu \text{ and } Z_\nu \text{ meet at a vertex with incoming momenta } p \text{ and } q, \text{ and outgoing } \phi \text{ bosons.} \\
& = -8i g_{\mu\nu} \left(\frac{C_{B\phi^2}}{\Lambda^2} \sin^2(\theta_w) p \cdot q \right. \\
& \quad \left. + \frac{C_{W\phi^2}}{\Lambda^2} \cos^2(\theta_w) p \cdot q \right) \\
& \quad + 8i \left(\frac{C_{B\phi^2}}{\Lambda^2} \sin^2(\theta_w) p_\nu q_\mu \right. \\
& \quad \left. + \frac{C_{W\phi^2}}{\Lambda^2} \cos^2(\theta_w) p_\nu q_\mu \right) \\
& \quad + 2i \frac{C_{(DH)^2\phi^2}}{\Lambda^2} g_{\mu\nu} m_Z^2 \\
& \text{Diagram 2: } G_0 \text{ and } Z_\mu \text{ meet at a vertex with incoming momenta } p \text{ and } q, \text{ and outgoing } \phi \text{ bosons.} \\
& = 2 \frac{C_{(DH)^2\phi^2} m_W}{\Lambda^2 \cos(\theta_W)} p_\mu
\end{aligned} \tag{2.25}$$

$$\begin{aligned}
& \text{Diagram 1: } H \text{ and } H \text{ meet at a vertex with incoming momenta } p \text{ and } q, \text{ and outgoing } \phi \text{ bosons.} \\
& = i \frac{6C_{H^4\phi^2}}{\Lambda^2} \left(\frac{2m_W}{g} \right)^2 \\
& \quad - 2i \frac{C_{(DH)^2\phi^2}}{\Lambda^2} p \cdot q \\
& \text{Diagram 2: } G_+ \text{ and } W_\mu^- \text{ meet at a vertex with incoming momenta } p \text{ and } q, \text{ and outgoing } \phi \text{ bosons.} \\
& = 2i \frac{C_{(DH)^2\phi^2} m_W}{\Lambda^2} p_\mu
\end{aligned} \tag{2.26}$$

$$\begin{aligned}
& \text{Diagram 1: } G_0 \text{ and } G_0 \text{ meet at a vertex with incoming momenta } p \text{ and } q, \text{ and outgoing } \phi \text{ bosons.} \\
& = 2i \frac{C_{H^4\phi^2}}{\Lambda^2} \left(\frac{2m_W}{g} \right)^2 \\
& \quad - 2i \frac{C_{(DH)^2\phi^2}}{\Lambda^2} p \cdot q \\
& \text{Diagram 2: } G_- \text{ and } W_\mu^+ \text{ meet at a vertex with incoming momenta } p \text{ and } q, \text{ and outgoing } \phi \text{ bosons.} \\
& = -2i \frac{C_{(DH)^2\phi^2} m_W}{\Lambda^2} p_\mu
\end{aligned} \tag{2.27}$$

Note that these are all effective interactions, originating from an EFT. Typically one would denote this with a striped bubble at the vertex. We omit this, to avoid confusion with the notation of the lower energy EFT we will define later.

2.3 Loop Calculations

Now we have determined the Feynman rules needed for $ee\phi\phi$ scattering at one-loop level, we can identify the relevant diagrams and amplitudes. Three generic structures can be identified, triangle one-loops diagrams, lollipop loop diagrams and tree level diagrams with an additional bubble.

$$A = \nu_e, (B, C) = \begin{cases} (W^+, W^-) \\ (G_+, W^-) \\ (W^+, G_-) \\ (G_+, G_-) \end{cases}$$

$$A = e, (B, C) = \begin{cases} (Z, Z) \\ (Z, G_0) \\ (G_0, G_0) \\ (G_0, Z) \\ (H, H) \end{cases} \quad (2.32)$$

$$D = H, (E, F) = \begin{cases} (H, H) \\ (Z, Z) \\ (Z, G_0) \\ (G_0, G_0) \\ (W^+, W^-) \\ (W^+, G_-) \\ (W^-, G_+) \\ (G_+, G_-) \end{cases} \quad (2.33)$$

The diagram shows a loop structure. At the top, two electron lines (e) meet at a vertex. The incoming electron has momentum k, and the outgoing electron has momentum p. A dashed line labeled H connects this vertex to a central black dot. From this dot, a dashed line labeled G goes to another vertex. From this second vertex, two phi lines emerge: one with momentum k2 and one with momentum p2. A loop is formed by a solid line connecting the central dot to the second vertex. Equation (2.34) is given as $H = H, G = \begin{cases} Z \\ W \end{cases}$.

These diagrams together form a complete set to match the Wilson coefficients $C_{(DH)^2\phi^2}, C_{W\phi^2}$ and $C_{B\phi^2}$ onto the lower energy DM EFT. In the first set, the particles (B, C) are defined as outgoing of the $\phi\phi$ vertex at the bottom. Note that only lollipop diagrams with $D = H$ contribute, diagrams with $D = G_0, Z$ vanish upon evaluation and hence will not contribute to the matching.

We also do not consider diagrams of type (2.34) for $G = G_+, G_0, H$, as these diagrams are only proportional to one Wilson coefficient: $C_{H^4\phi^2}$. Later, we will see that there is a $C_{H^4\phi^2}$ contribution at tree level. As our aim is to research what terms arise first at one-loop order, we are not interested in NLO corrections to $C_{H^4\phi^2}$, and such corrections would also not be complete in our study. Later we will discard the $C_{H^4\phi^2}$ contributions, so this would mean that the amplitudes of all diagrams with $G = G_+, G_0, H$ would be removed anyway. We thus opt to not calculate these diagrams.

When performing the loop calculations, we first export the DSMEFT Feynman rules from FeynArts, to create a custom model for the Mathematica package FeynArts [34]. We then use FeynArts to generate the loop diagrams and amplitudes of (2.32,2.33,2.34). Note that one must explicitly define that vertices with an adjacency of 5 are allowed when generating the diagrams. Otherwise, the diagrams of the third type are not generated in FeynArts.

Further computations are performed by Mathematica Package FeynCalc [30]. The electrons are not set on-shell, as they are bound in noble gas atoms in direct detection experiments. These bound electrons are not close to momentum-eigenstates, with typical momentum scales of $p_0 \equiv 1/a_0 = 3.73$ keV, a_0 being the Bohr radius. The ionisation energy of electrons in the outer shell of noble gas atoms are in the order of 10 eV. From this, one can infer that $|\vec{k}|, |\vec{p}| \ll m_e$ for electron excitations. Even in this situation, one cannot set the electrons on-shell, as this does not correspond to the reality of the experimental context, where the framework of individual excitations does not apply. One can for example possibly encounter double excitations [35]. For generality, it is thus appropriate to work in a scenario with off-shell electrons.

Additionally, we note both the external momenta and m_e are much smaller than the mass of the

heavy loop particles with $M = m_Z, m_W, m_H$. We can thus use the fact that $m_e, p, k \ll M$, with M being any of the heavy loop particles. The goal is now to calculate the loop amplitudes of the above diagrams up to the leading order of m_e/M . Higher orders of m_e/M are discarded.

Before performing the loop integration by means of Passarino-Veltman tensor integral reduction, we expand the propagators. Recall that a general denominator for loops such as those given by (2.32) is

$$\frac{1}{(l^2 - m_A^2)((l-k)^2 - M_B^2)((l-p)^2 - M_C^2)} \quad (2.35)$$

This expansion is again motivated by the fact that the energy scales of the internal loop particles are much higher than the energy scales of m_e and the external momenta k, p . To obtain the full result up to the leading order in m_e , one needs to carefully assess this expansion. The triangle loops with internal particles (e, G_0, G_0) , (e, H, H) and (ν_e, G_+, G_-) already contain at least two insertions of m_e , due to two occurrences of the Higgs to electron coupling. In these cases the propagators thus only need to be expanded up to the zeroth order in p and k :

$$\frac{1}{((l-k)^2 - M^2)((l-p)^2 - M^2)(l^2 - m^2)} \approx \frac{1}{l^2} \frac{1}{(l^2 - M^2)^2} \quad (2.36)$$

For the remaining triangle loops, we must expand the propagator one step deeper to obtain all the leading order m_e terms:

$$\begin{aligned} \frac{1}{(l^2 - m^2)((l-k)^2 - M^2)((l-p)^2 - M^2)} &= \frac{1}{(l^2 - m^2)} \frac{1}{(l^2 - M^2)} \left[\frac{1}{1 - \frac{2l \cdot k - k^2}{(l^2 - M^2)}} \right] \\ &\cdot \frac{1}{(l^2 - M^2)} \left[\frac{1}{1 - \frac{2l \cdot p - p^2}{(l^2 - M^2)}} \right] \end{aligned} \quad (2.37)$$

$$\approx \frac{1}{l^2(l^2 - M^2)^2} \left[1 + 2 \frac{l \cdot p + l \cdot k}{(l^2 - M^2)} \right] \quad (2.38)$$

where we have used the geometric series $\sum_{n=0}^{\infty} x^n = \frac{1}{1-x}$ for $x < 1$ in the final line. We only retain terms up to order 1 in p and k in the numerator. Note that we only denote two masses in this expansion: m and M . Here m refers to particle A in the triangle loop, such that either $m = m_e$ or $m = 0$, for $A = \nu_e$. We only need to introduce one additional heavy mass M , rather than distinguish between M_B and M_C , due to the fact that all the calculated triangle loops contain only one heavy mass in their loop integrand.

In the cases where we do not obtain two identical particles in the loop, we have a gauge boson and its corresponding longitudinal mode, the Goldstone boson. The propagators of these Goldstone bosons contain the mass corresponding to its respective gauge boson, giving two insertions of $M = m_Z$ for $(A, B, C) = (e, Z, G_0)$ for example. Similar expansions can be made for the lollipop loops. Note that, again, we need to distinguish between only two masses, m_H and M in this case.

$$\frac{1}{((p-k)^2 - m_H^2)(l^2 - M^2)((l-k+p)^2 - M^2)} \approx \frac{1}{(-m_H^2)} \frac{1}{(l^2 - M^2)} \frac{1}{(l^2 - M^2)} \left[\frac{1}{1 - \frac{2(l \cdot k - l \cdot p)}{(l^2 - M^2)}} \right]$$

$$\approx \frac{-1}{(m_H^2)(l^2 - M^2)^2} \left[1 + 2 \frac{l \cdot k - l \cdot p}{(l^2 - M^2)} \right] \quad (2.39)$$

Finally, the third type of loop diagram given in (2.34) can be rewritten as:

$$\frac{1}{(l^2 - M^2)((k - p)^2 - m_H^2)} \approx \frac{-1}{m_H^2(l^2 - M^2)} \quad (2.40)$$

with M being the mass of the heavy loop particle. We do not need to expand this denominator further, as further expansion would only give us terms of order two in p, k , which are not relevant for our calculations

After we have implemented the expansion of the amplitudes, we perform the Passarino-Veltman reduction in D dimensions. This leaves us with solely the scalar functions $A_0(M^2)$, $B_0(0, M^2, M^2)$ and $C_0(0, 0, 0, M^2, M^2, M^2)$, with M being the heavy loop particle mass. The analytical expressions for these scalar functions are easily obtained and can be cross-checked with the Mathematica package Package-X [31, 32]. We rewrite the amplitude by using the following relations.

$$A_0(M^2) = M^2(B_0(0, M^2, M^2) + 1) \quad (2.41)$$

$$(D - 4)B_0(0, M^2, M^2) = -2 \quad (2.42)$$

$$C_0(0, 0, 0, M^2, M^2, M^2) = -\frac{1}{2M^2} \quad (2.43)$$

Note that $B_0(0, M^2, M^2)$ contains a UV divergence. Before being able to set $D = 4$, we must apply (2.42).

The rewritten amplitude contains a finite, scalar part and, if present, a divergent part proportional to B_0 . The goal is to find the leading order contributions, by expanding the amplitude up to order one in m_e . Contributions proportional to m_e^N , with $N > 1$, are discarded. It is important to note that both the external momenta p and k , and m_e are of the same order of magnitude. If we were to expand all three terms separately, the order of expansion would influence the final results. To prevent this from happening, we introduce the following ratios:

$$RP = \frac{p^2}{m_e^2} \quad (2.44)$$

$$RK = \frac{k^2}{m_e^2} \quad (2.45)$$

$$RPK = \frac{p \cdot k}{m_e^2} \quad (2.46)$$

$$RM = \frac{m_e}{M} \quad (2.47)$$

with M being the relevant heavy loop particle mass for the amplitude in question. The ratios RP , RK and RPK are of order 1 for typical momentum transfers in DM-electron scattering. The amplitude is then expanded only in RM , as $RM \ll 1$. We expand RM up to order 1 to obtain the leading order terms up to order m_e .

2.3.1 DSMEFT Loop Amplitude Results

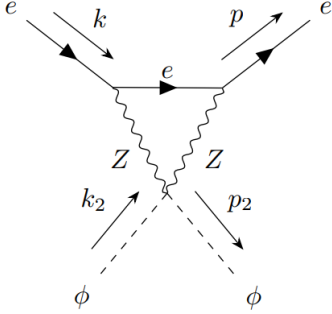
We now summarise the results of the loop amplitudes given by (2.32,2.33) after applying the procedure described above. Earlier on, we have stated that the electrons that are scattered in direct detection are bound in atoms, making them off-shell. To obtain more realistic results, one should find the amplitudes of the loop diagrams for the off-shell scenario, so without applying the Dirac equation.

We here give both the off-shell and on-shell amplitudes. When calculating the off-shell amplitudes, we find that only the (ν_e, W^+, W^-) and (e, Z, Z) triangle loop amplitudes are altered by implementing the on-shell condition. Both results are given for completeness, with (2.50,2.52) giving the off-shell amplitudes and (2.51,2.53) giving the on-shell amplitudes. In the results of the off-shell amplitudes, $\bar{\gamma}^6, \bar{\gamma}^7$ refer to the right and left handed projection operators:

$$\bar{\gamma}^6 = \frac{1}{2}(1 + \gamma^5) \quad (2.48)$$

$$\bar{\gamma}^7 = \frac{1}{2}(1 - \gamma^5) \quad (2.49)$$

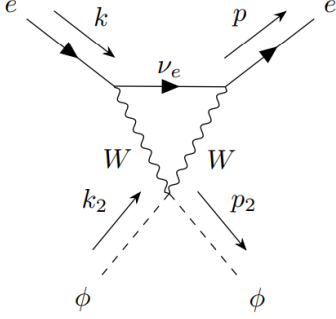
Note that all other types of diagram amplitudes are identical for the on and off-shell cases, as the Higgs boson yields a scalar interaction. The amplitudes given below thus give the full result for off-shell electrons.



$$\begin{aligned} \text{off-shell} \quad & i \frac{e^2 \tan^2(\theta_W) e^2}{64\pi^2 \Lambda^2} \left\{ [(C_{B\phi^2} - C_{W\phi^2}) \cos(2\theta_W) - C_{B\phi^2} - C_{W\phi^2}] \right. \\ & \cdot \left[\frac{3 \cos^2(2\theta_W) (\not{p} + \not{k}) \cdot \bar{\gamma}^7}{\sin(\theta_W)^4} \right. \\ & \left. \left. + 12 (\not{p} + \not{k}) \cdot \bar{\gamma}^6 - 8(3B_0(0, m_Z^2, m_Z^2) - 2)m_e \left(\frac{\cos(\theta_W)^2}{\sin(\theta_W)^2} - 1 \right) \right] \right. \\ & \left. - C_{(DH)^2\phi^2} \left[\frac{\cos^2(2\theta_W) (\not{p} + \not{k}) \cdot \bar{\gamma}^7}{\sin(\theta_W)^4} + 4 (\not{p} + \not{k}) \cdot \bar{\gamma}^6 \right. \right. \\ & \left. \left. + 16m_e \left(\frac{\cos(\theta_W)^2}{\sin(\theta_W)^2} - 1 \right) \right] \right\} \quad (2.50) \end{aligned}$$

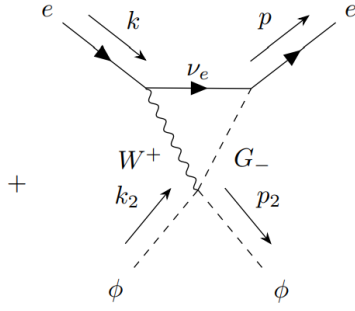
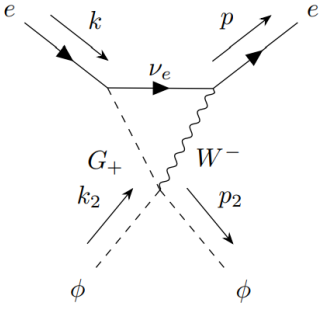
$$\begin{aligned} = & i \frac{e^2 m_e}{64\pi^2 \Lambda^2 \sin(\theta_W)^2 \cos(\theta_W)^2} \left\{ [(2 - 12B_0(0, m_Z^2, m_Z^2)) \cos(2\theta_W) \right. \\ & \left. + (6B_0(0, m_Z^2, m_Z^2) - 1) \cos(4\theta_W) + 6B_0(0, m_Z^2, m_Z^2) + 2] \right\} \end{aligned}$$

$$\cdot \left[(C_{B\phi^2} - C_{W\phi^2}) \cos(2\theta_W) - C_{B\phi^2} - C_{W\phi^2} \right] + C_{(DH)^2\phi^2} \left(-6 \cos(2\theta_W) + 3 \cos(4\theta_W) + 2 \right) \} \quad (2.51)$$



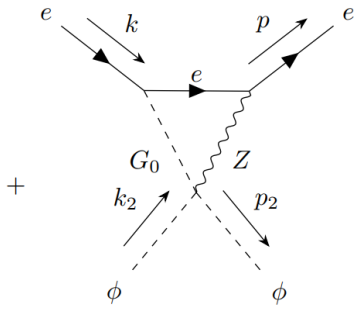
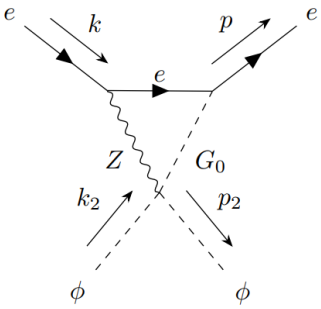
$$\stackrel{\text{off-shell}}{=} -i \frac{e^2}{32\pi^2 \Lambda^2 \sin(\theta_W)^2} (C_{(DH)^2\phi^2} + 6C_{W\phi^2}) \left((\not{p} + \not{k}) \cdot \bar{\gamma}^7 \right) \quad (2.52)$$

$$= -i \frac{e^2 m_e}{32\pi^2 \Lambda^2 \sin(\theta_W)^2} (C_{(DH)^2\phi^2} + 6C_{W\phi^2}) \quad (2.53)$$



$$= -i \frac{C_{(DH)^2\phi^2} e^2 m_e}{16\pi^2 \Lambda^2 \sin(\theta_W)^2} B_0(0, m_W^2, m_W^2)$$

$$(2.54)$$



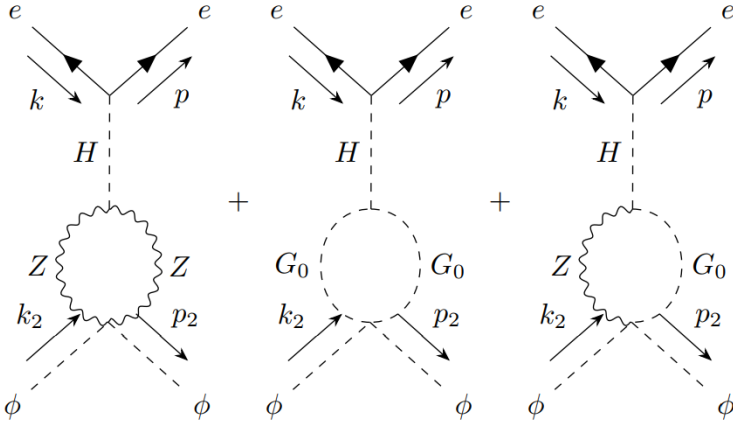
$$= -i \frac{C_{(DH)^2\phi^2} e^2 m_e}{8\pi^2 \Lambda^2 \sin(2\theta_W)^2} B_0(0, m_Z^2, m_Z^2)$$

$$(2.55)$$

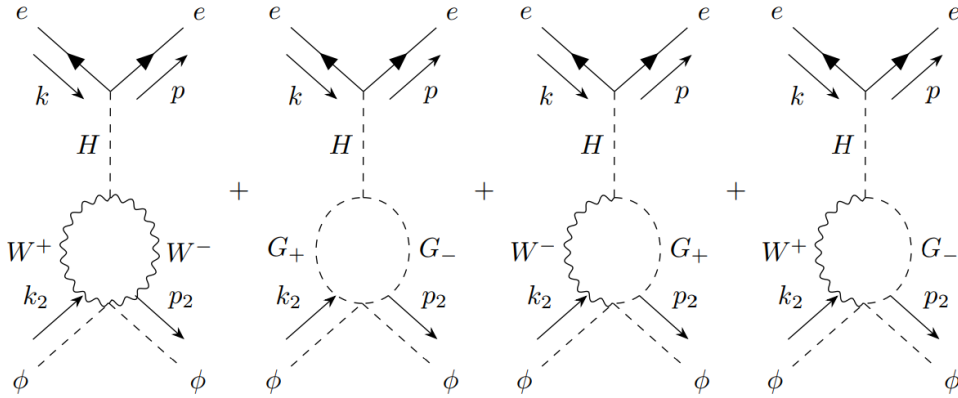
$$= 0 \quad (2.56)$$

$$= 0 \quad (2.57)$$

$$= 6i \frac{C_{(DH)^2 \phi^2} e^2 m_e m_H^2}{16\pi^2 \sin^2(2\theta_W) m_Z^2} \left(B_0(0, m_H^2, m_H^2) + \frac{1}{2} \right) + 9i \frac{C_{H^4 \phi^2} m_Z^2}{16\pi^2 \Lambda^2 m_Z^2} B_0(0, m_H^2, m_H^2) \quad (2.58)$$



$$\begin{aligned}
&= -\frac{i e^2 m_e m_Z^2}{8\pi^2 \cos(\theta_W)^2 \Lambda^2 \sin(\theta_W)^2 m_H^2} (C_{B\phi^2} \sin(\theta_W)^2 + \cos(\theta_W)^2 C_{W\phi^2}) (6B_0(0, m_Z^2, m_Z^2) - 1) \\
&+ \frac{i C_{(DH)^2\phi^2} e^2 m_e}{64\pi^2 \cos(\theta_W)^2 \Lambda^2 \sin(\theta_W)^2 m_H^2} \left((2B_0(0, m_Z^2, m_Z^2) + 1) m_H^2 + 2(3 - 2B_0(0, m_Z^2, m_Z^2)) m_Z^2 \right) \\
&+ \frac{i C_{H^4\phi^2} m_e}{16\pi^2 \Lambda^2} B_0(0, m_Z^2, m_Z^2) \tag{2.59}
\end{aligned}$$



$$\begin{aligned}
&= \frac{i C_{(DH)^2\phi^2} e^2 m_e}{32\pi^2 \Lambda^2 \sin(\theta_W)^2 m_H^2} \left(2(3 - 2B_0(0, m_W^2, m_W^2)) \cos(\theta_W)^2 m_Z^2 + (2B_0(0, m_W^2, m_W^2) + 1) m_H^2 \right) \\
&+ \frac{i B_0(0, m_W^2, m_W^2) C_{H^4\phi^2} m_e}{8\pi^2 \Lambda^2} \tag{2.60}
\end{aligned}$$

$$-\frac{i \cos(\theta_W)^2 C_{W\phi^2} e^2 m_e m_Z^2}{4\pi^2 \Lambda^2 \sin(\theta_W)^2 m_H^2} (6B_0(0, m_W^2, m_W^2) - 1) \tag{2.61}$$

$$\begin{aligned}
&= -i \frac{e^2 m_e C_{(DH)^2 \phi^2}}{16\pi^2 \Lambda^2 \sin^2(\theta_W) m_H^2} \left[4m_W^2 \left(B_0(0, m_W^2, m_W^2) + \frac{1}{2} \right) + \frac{2m_Z^2}{\cos^2(\theta_W)} \left(B_0(0, m_Z^2, m_Z^2) + \frac{1}{2} \right) \right] \\
&\hspace{20em} (2.62)
\end{aligned}$$

The scalar integral $B_0(0, M^2, M^2)$ is given by

$$B_0(0, M^2, M^2) \equiv \left(\log \left(\frac{\mu^2}{M^2} \right) - \gamma + \log(4\pi) + \frac{1}{\epsilon} \right) \quad (2.63)$$

where we define $\epsilon = (4-D)/2$. All amplitudes contain only Lorentz scalar structures, with the exception of the off-shell amplitudes (2.52, 2.50). We shall now continue with only the scalar amplitudes, indicating that we are implementing on-shell conditions for the scattered electrons.

We can now combine all the loop amplitudes into one expression, collecting all terms per Wilson coefficient. This gives us the following result for the next to leading order (NLO) amplitude for loop induced DM-electron interactions with on-shell electrons:

$$\begin{aligned}
\mathcal{A}_{NLO} = & i \frac{m_e}{128\pi^2 \Lambda^2} \left[\frac{4e^2}{m_H^2 m_Z^2} \left\{ \frac{6(2B_0(0, m_H^2, m_H^2) + 1)C_{(DH)^2 \phi^2} m_H^4}{\sin^2(2\theta_W)} \right. \right. \\
& + m_Z^4 \left(-\frac{3(4B_0(0, m_W^2, m_W^2) + 2B_0(0, m_Z^2, m_Z^2) - 1)(C_{(DH)^2 \phi^2} + 4C_W \phi^2)}{\sin^2(\theta_W)} \right. \\
& + 2(6B_0(0, m_W^2, m_W^2) - 1)(C_{(DH)^2 \phi^2} + 4C_W \phi^2) - \frac{(6B_0(0, m_Z^2, m_Z^2) - 1)(4C_{B\phi^2} + C_{(DH)^2 \phi^2})}{\cos^2(\theta_W)} \\
& + m_H^2 m_Z^2 \left(\frac{-24B_0(0, m_Z^2, m_Z^2)C_{B\phi^2} + C_{B\phi^2} + 6C_{(DH)^2 \phi^2}}{\cos^2(\theta_W)} - 8C_{B\phi^2} - 12C_{(DH)^2 \phi^2} \right. \\
& \left. \left. - 4(6B_0(0, m_Z^2, m_Z^2) - 1)(C_{B\phi^2} - C_W \phi^2) \cos(2\theta_W) + 48B_0(0, m_Z^2, m_Z^2)C_{B\phi^2} - \frac{9C_W \phi^2}{\sin^2(\theta_W)} \right) \right. \\
& \left. + 8C_{H^4 \phi^2} \left(9B_0(0, m_H^2, m_H^2) + 2B_0(0, m_W^2, m_W^2) + B_0(0, m_Z^2, m_Z^2) \right) \right] \quad (2.64)
\end{aligned}$$

This amplitude still contains an insertion of $C_{H^4 \phi^2}$. As we will see, this Wilson coefficient already contributes at tree level. Our interest lies in the Wilson coefficients that first contribute at one-loop

level. For completeness, we have thus given the first result of \mathcal{A}_{NLO} with the inclusion of $C_{H^4\phi^2}$, but it shall from now on be removed from the total amplitude. Additionally, we notice that these amplitudes are divergent, due to the inclusion of the B_0 terms. It is thus necessary to renormalise our DSMEFT Lagrangian so that the obtained loop amplitudes are finite. We shall discuss this in section 2.4.

2.4 Renormalisation

When we obtained the total amplitude of all diagrams that will be relevant for our DSMEFT matching, we noticed that \mathcal{A}_{NLO} contains UV divergences $1/\epsilon$, introduced by the scalar two-point integrals $B_0(0, M^2, M^2)$. Before we proceed with the matching of DSMEFT with a lower energy theory, we need to remove these divergences from the total amplitude by means of renormalisation. Renormalisation is an analytical procedure that allows one to remove divergences from loop diagram by introducing a limited amount of redefinitions in the Lagrangian of a theory.

Renormalisation is an application based method, as different approaches can be chosen, based on the theory at hand. Generally sketched, the procedure is performed as follows. First, the non-renormalised, bare, Lagrangian \mathcal{L}_0 is written down. The parameters that need to be renormalised are then rewritten in terms of the renormalised ones. The exact redefinition is based on the renormalisation scheme that is chosen. Depending on the used theory, one needs to renormalise the fields, masses or couplings, or a combination of these. These renormalised parameters give rise to so-called counterterms, which introduce additional Feynman rules that absorb the divergences. Note that renormalisation is always performed at a chosen renormalisation scale μ_R .

We now rewrite (2.64), in order to obtain an expression that isolates the divergent elements. Note that the superscript (0) indicates that this is the so-called bare amplitude, as it is not renormalised yet. Note that we are thus renormalising the DSMEFT.

$$\begin{aligned}
\mathcal{A}_{NLO}^{(0)} = & i \frac{e^2 m_e}{128\pi^2 m_H^2 m_Z^2 \cos(\theta_W)^2 \Lambda^2} \left[C_{(DH)^2\phi^2} \left(\frac{12B_0(0, m_H^2, m_H^2) m_H^4}{\sin(\theta_W)^2} \right. \right. \\
& - \frac{48B_0(0, m_W^2, m_W^2) \cos^2(\theta_W) \cos(\theta_W)^2 m_Z^4}{\sin(\theta_W)^2} - \frac{24B_0(0, m_Z^2, m_Z^2) m_Z^4}{\sin(\theta_W)^2} \\
& + \frac{6m_H^4}{\sin(\theta_W)^2} - 24m_H^2 \cos(2\theta_W) m_Z^2 + \frac{(4 \cos(2\theta_W) + \cos(4\theta_W) + 7)m_Z^4}{\sin(\theta_W)^2} \Big) \\
& + C_{W\phi^2} \left(- \frac{192B_0(0, m_W^2, m_W^2) \cos^2(\theta_W) \cos(\theta_W)^2 m_Z^4}{\sin(\theta_W)^2} \right. \\
& + 96B_0(0, m_Z^2, m_Z^2) m_Z^2 \left(m_H^2 \cos^2(\theta_W) \cos(2\theta_W) - \frac{\cos(\theta_W)^2 m_Z^2}{\sin(\theta_W)^2} \right) \\
& \left. \left. + \frac{4 \cos(\theta_W)^2 m_Z^2 (m_H^2 (-2 \cos(2\theta_W) + \cos(4\theta_W) - 8) + 4(\cos(2\theta_W) + 2)m_Z^2)}{\sin(\theta_W)^2} \right) \right)
\end{aligned}$$

$$\begin{aligned}
& + C_{B\phi^2} \left(4m_Z^2 (m_H^2 (-2\cos(2\theta_W) + \cos(4\theta_W) - 2) + 4m_Z^2) \right. \\
& \left. - 96B_0(0, m_Z^2, m_Z^2)m_Z^2 (m_Z^2 - m_H^2 \sin^2(\theta_W) \cos(2\theta_W)) \right) \Big] \tag{2.65}
\end{aligned}$$

Due to our choice to set the amplitudes of the triangle loops (ν_e, W^+, W^-) and (e, Z, Z) on-shell, we obtain a fully scalar amplitude. The counterterm that will absorb the divergent part of the diagram of (2.65) is of $(\bar{L}_L^i H e_R^i)\phi\phi$ structure, due to the scalar nature of the total amplitude. We must thus renormalise our theory in such a way that the $\frac{C_{e\phi}}{\Lambda^2}(\bar{L}_L^i H e_R^i)\phi\phi$ term in our DSMEFT Lagrangian absorbs the divergent parts of \mathcal{A}_{NLO} . Remark that $C_{H^4\phi^2}$ could in principle absorb the divergences of the lollipop diagrams through the $H\phi\phi$ vertex. This would be a different way to describe the same physics, so here we choose to absorb all divergences, including those originating from the lollipop diagrams, in the $C_{e\phi^2}$ coefficient. Additionally, we will integrate out the Higgs in our lower energy theory, DLEFT, so it is more efficient to directly absorb all divergences in the $ee\phi\phi$ vertex.

So, in this specific case, only a renormalisation of the Wilson coefficient $C_{e\phi^2}$ is necessary. The self-energies of the Higgs boson and the DM scalar ϕ do not give a contribution to the wave function renormalisation factors at one-loop level for the amplitudes we consider, as they do not contain terms proportional to p^2, k^2 . The DM mass m_ϕ is also not a parameter that occurs in the considered amplitudes. So, solely the Wilson coefficient $C_{e\phi^2}$ needs to be rewritten in its renormalised terms. We define our bare Wilson Coefficients as $C_X^{(0)}$, with subscript X denoting the specific Wilson coefficient. We can treat the Wilson coefficients as couplings, and renormalise them on a coefficient by coefficient basis. Notice that we generate a renormalised coefficient $\mathcal{C}_{e\phi^2}$ through loop diagrams with insertions of $C_{H^4\phi^2}, C_{(DH)^2\phi^2}, C_{W\phi^2}$ and $C_{B\phi^2}$. We are thus dealing with coupling mixing, and we need to express our renormalisation constant as a matrix \hat{Z}_C that contains off-diagonal elements.[36]

$$\begin{pmatrix} C_{e\phi^2}^{(0)} \\ C_{(DH)^2\phi^2}^{(0)} \\ C_{W\phi^2}^{(0)} \\ C_{B\phi^2}^{(0)} \end{pmatrix} = \hat{Z}_C \begin{pmatrix} C_{e\phi^2} \\ C_{(DH)^2\phi^2} \\ C_{W\phi^2} \\ C_{B\phi^2} \end{pmatrix} \tag{2.66}$$

Let us now further examine the term in our DSMEFT Lagrangian that will provide the counterterm to absorb the divergences of the NLO contributions. We start from the Lagrangian \mathcal{L} with bare coefficient $C_{e\phi^2}^{(0)}$ and use (2.66) to rewrite in terms of the renormalised Wilson coefficient. All renormalised coefficients are defined at the renormalisation scale μ_R , such that from this point onwards, $C \equiv C(\mu_R)$. For readability we do not explicitly write down the μ_R dependence for every

Wilson coefficient C , but all renormalised coefficients are defined at this scale.

$$\begin{aligned}
\mathcal{L}(\mu_R) &= \frac{C_{e\phi^2}^{(0)}}{\Lambda^2} \phi\phi\bar{L}He_R \\
&= \frac{Z_{11}C_{e\phi^2} + Z_{12}C_{(DH)^2\phi^2} + Z_{13}C_{W\phi^2} + Z_{14}C_{B\phi^2}}{\Lambda^2} \phi\phi\bar{L}He_R \\
&= \frac{C_{e\phi^2} + \delta_{12}C_{(DH)^2\phi^2} + \delta_{13}C_{W\phi^2} + \delta_{14}C_{B\phi^2}}{\Lambda^2} \phi\phi\bar{L}He_R
\end{aligned} \tag{2.67}$$

Here μ_R denotes the renormalisation scale. In the last line we have used the relation $Z_{11} = 1$, as we do not need to renormalise the coefficient $C_{e\phi^2}$, as it does not occur in \mathcal{A}_{NLO} . Furthermore, coupling mixing only occurs at loop level and there is thus no tree-level contribution to the renormalisation of the remaining wilson coefficients, allowing us to define $Z_{ij} = \delta_{ij}$ for all $i \neq j$.

The goal now is to define δ_{12} through δ_{14} such that the divergence of the diagram is absorbed at a chosen renormalisation scale μ_R , leaving us with a finite amplitude. In the context of the Dark Matter EFT used here, we set the renormalisation scale μ_R to the EFT cutoff scale Λ , which corresponds to the electroweak scale $v \approx 246$ GeV. In addition, we must choose a convenient renormalisation scheme. In the Minimal Subtraction (MS) scheme, only the divergent pole $\frac{1}{\epsilon}$ is absorbed. In our case, the pole is always accompanied by $\log(\mu^2)$, the Euler constant γ and $\log(4\pi)$. We can thus absorb

$$\frac{1}{\hat{\epsilon}} = \frac{1}{\epsilon} - \gamma + \log(4\pi) + \log\left(\frac{\mu^2}{\mu_R^2}\right) \tag{2.68}$$

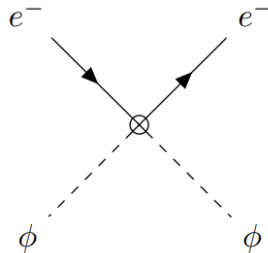
in our counterterm, which is referred to as the \overline{MS} scheme.[37] We can now combine (2.65) with (2.66) to identify the counterterms from the divergent parts of the amplitude.

$$\delta_{12} = -\frac{3}{4} \left[\frac{m_H^4}{\sin(\theta_W)^2} - 2m_Z^4 \left(\frac{2\cos^2(\theta_W)\cos(\theta_W)^2 + 1}{\sin(\theta_W)^2} \right) \right] \left[\frac{1}{\epsilon} - \gamma + \log(4\pi) + \log\left(\frac{\mu^2}{\mu_R^2}\right) \right] \tag{2.69}$$

$$\begin{aligned}
\delta_{13} &= -6 \left[m_H^2 m_Z^2 \cos(\theta_W)^2 \cos(2\theta_W) - \frac{(\cos(2\theta_W) + 2)\cos(\theta_W)^2 m_Z^4}{\sin(\theta_W)^2} \right] \\
&\quad \cdot \left[\frac{1}{\epsilon} - \gamma + \log(4\pi) + \log\left(\frac{\mu^2}{\mu_R^2}\right) \right]
\end{aligned} \tag{2.70}$$

$$\delta_{14} = 6m_Z^2 \left[m_Z^2 - m_H^2 \sin(\theta_W)^2 \cos(2\theta_W) \right] \left[\frac{1}{\epsilon} - \gamma + \log(4\pi) + \log\left(\frac{\mu^2}{\mu_R^2}\right) \right] \tag{2.71}$$

Here we have pulled out an overall factor $\frac{e^2 m_e}{16\pi^2 m_H^2 m_Z^2 \cos(\theta_W)^2 \Lambda^2}$. We can now determine the new Feynman rule that contains the counterterms



$$\begin{aligned}
&= i \frac{2e^2 m_e}{16\pi^2 m_H^2 m_Z^2 \cos(\theta_W)^2 \Lambda^2} \left(\delta_{12} C_{(DH)^2\phi^2} \right. \\
&\quad \left. + \delta_{13} C_{W\phi^2} + \delta_{14} C_{B\phi^2} \right)
\end{aligned} \tag{2.72}$$

where we have defined the counterterms δ_{1j} , with $j=2,3,4$, using (2.69-2.71). This new Feynman rule absorbs the divergences in our amplitude $\mathcal{A}_{NLO}(\mu_R)$. Now we can define the finite total amplitude that remains after normalisation. Remember that all Wilson coefficients are defined at the renormalisation scale μ_R . Additionally, the undefined scale of μ is now effectively set to our chosen renormalisation scale μ_R . So, by performing the renormalisation, we additionally fix the value of μ to μ_R . In our case, we set μ_R to be in the range of the weak scale, which we shall return to in section 2.6.

$$\begin{aligned}
\mathcal{A}_{NLO}(\mu_R) = & i \frac{e^2 m_e}{32\pi^2 m_H^2 m_Z^2 \Lambda^2} \left[\frac{6(2 \log\left(\frac{\mu_R^2}{m_H^2}\right) + 1) C_{(DH)^2 \phi^2} m_H^4}{\sin(2\theta_W)^2} \right. \\
& + m_Z^4 \left(- \frac{3(4 \log\left(\frac{\mu_R^2}{m_W^2}\right) + 2 \log\left(\frac{\mu_R^2}{m_Z^2}\right) - 1)(C_{(DH)^2 \phi^2} + 4C_{W\phi^2})}{\sin(\theta_W)^2} \right. \\
& + 2(6 \log\left(\frac{\mu_R^2}{m_W^2}\right) - 1)(C_{(DH)^2 \phi^2} + 4C_{W\phi^2}) - \frac{(6 \log\left(\frac{\mu_R^2}{m_Z^2}\right) - 1)(4C_{B\phi^2} + C_{(DH)^2 \phi^2})}{\cos(\theta_W)^2} \Big) \\
& + m_H^2 m_Z^2 \left(\frac{\cos(2\theta_W)(4(6 \log\left(\frac{\mu_R^2}{m_Z^2}\right) - 1)C_{B\phi^2} - 6C_{(DH)^2 \phi^2}) - 3C_{B\phi^2}}{\cos(\theta_W)^2} \right. \\
& \left. \left. - 4(6 \log\left(\frac{\mu_R^2}{m_Z^2}\right) - 1)(C_{B\phi^2} - C_{W\phi^2}) \cos(2\theta_W) - \frac{9C_{W\phi^2}}{\sin(\theta_W)^2} \right) \right] \tag{2.73}
\end{aligned}$$

$$(2.74)$$

The $\log(\mu_R^2/M^2)$ are finite terms originating from $B_0(0, M^2, M^2)$.

2.5 DLEFT Operators

Now we have obtained all amplitudes from our DSMEFT Lagrangian, we proceed to our Dark Low Energy Effective Field Theory (DLEFT). The DLEFT is obtained by integrating out all particles with electroweak-scale masses, namely the top quark t , the W^\pm, H and Z bosons. When working with the lower energies relevant for DLEFT, one must keep in mind that the momentum transfer q and electron mass m_e cannot be ignored or set to zero. Our DM scalar follows the same conventions as those stated in Section 2.1 and we again base our DLEFT operators on [2]. First we identify all relevant operators in Table 2.1.

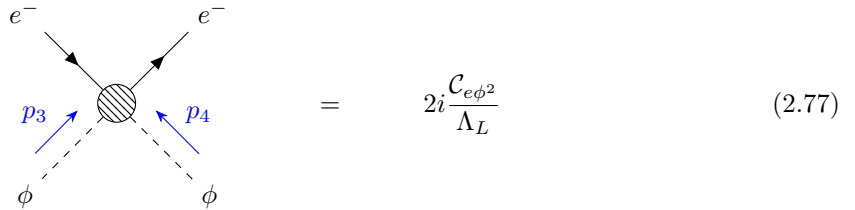
Name	Operator	Dimension (d_{SM}, d_{DM})
$\mathcal{O}_{e\phi^2}$	$(\bar{e}_L^i e_R^i)\phi^2$	(3, 2)
$\mathcal{O}_{F\phi^2}$	$F_{\mu\nu}F^{\mu\nu}\phi^2$	(4, 2)
$\mathcal{O}_{\tilde{F}\phi^2}$	$\tilde{F}_{\mu\nu}F^{\mu\nu}\phi^2$	(4, 2)

Table 2.1: DLEFT operators relevant for scalar DM scattering off an electron. Here j refers to the generation label. Additionally, d_{SM}, d_{DM} are the Standard Model and Dark Matter mass dimension.

Here we use

$$e_{L/R,j} = P_{L/R}e_j = \frac{1}{2}(1 - / + \gamma^5)e_j \quad (2.75)$$

$$\bar{e}_{L/R,j} = \bar{e}_j P_{R,L} = \bar{e}_j \frac{1}{2}(1 + / - \gamma^5) \quad (2.76)$$



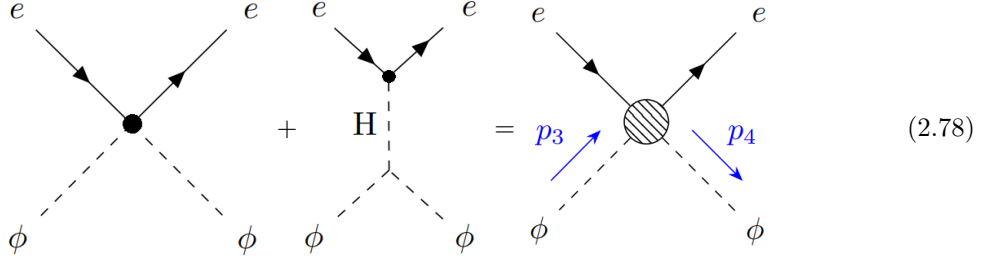
$$= 2i \frac{\mathcal{C}_{e\phi^2}}{\Lambda_L} \quad (2.77)$$

2.6 Matching DSMEFT with DLEFT

2.6.1 Tree Level Matching

At the start of this chapter, we have stated that our goal is to match the Wilson coefficients of the higher energy theory (DSMEFT) to the coefficients of the lower energy theory (DLEFT). We perform the matching by studying $e\phi \rightarrow e\phi$ scattering. Before we apply the full one-loop matching, we describe the matching between our DSMEFT and DLEFT theories at leading order (LO).

At high energies the tree level amplitude of the electron-DM process has contributions of two diagrams: a $ee\phi\phi$ vertex and a tree diagram with a Higgs boson propagator. The Feynman rule given in (2.77) gives the amplitude for the effective scattering diagram at energies below the weak scale. The amplitudes of the following diagrams are relevant for the tree level matching procedure, with the DSMEFT diagrams on the left hand side, and the DLEFT diagram on the right hand side:



First, we find the the total amplitude of the lefthand side of (2.78).

$$\mathcal{A}_{LO} = i \frac{2C_{e\phi} m_e}{\Lambda^2} + i \frac{8C_{H^4\phi^2} m_e m_W^2 \sin(\theta_W)^2}{e^2 \Lambda^2 (q^2 - m_H^2)} \quad (2.79)$$

$$= i \frac{2C_{e\phi} m_e}{\Lambda^2} - i \frac{8C_{H^4\phi^2} m_e m_W^2 \sin(\theta_W)^2}{e^2 \Lambda^2 m_H^2} \quad (2.80)$$

We have used that $q \equiv p - k$, with k and p respectively being the incoming and outgoing momenta of the electron. In the second line we have used the fact that $q^2 \ll m_H^2$, as we are working in the context of direct detection, where q is of sub-MeV order. Note that \mathcal{A}_{NLO} is fully scalar, we thus only need to match onto the scalar part of (2.77), the term that is proportional to $\mathcal{C}_{e\phi^2}$. We can now combine (2.80) with (2.77) to express the DLEFT Wilson coefficient $\mathcal{C}_{e\phi^2}$ in terms of DSMEFT coefficients:

$$\frac{2\mathcal{C}_{e\phi^2}}{\Lambda_L} = \frac{2C_{e\phi} m_e}{\Lambda^2} - \frac{8C_{H^4\phi^2} m_e m_W^2 \sin(\theta_W)^2}{e^2 \Lambda^2 m_H^2} \quad (2.81)$$

$$\mathcal{C}_{e\phi^2}^{LO}(\mu_M) = \frac{\Lambda_L m_e}{\Lambda^2} \left[C_{e\phi^2}(\mu_M) - \frac{4C_{H^4\phi^2}(\mu_M) m_W^2 \sin(\theta_W)^2}{e^2 m_H^2} \right] \quad (2.82)$$

$$\mathcal{C}_{e\phi^2}^{LO}(\mu_M) = \frac{\Lambda_L m_e}{\Lambda^2} \left[C_{e\phi^2}(\mu_M) - \frac{C_{H^4\phi^2}(\mu_M) v^2}{m_H^2} \right] \quad (2.83)$$

where in the last line we have used the relation $m_W^2 = e^2 v^2 / 4 \sin(\theta_W)^2$. Remark that the coefficients with a C refer to DSMEFT coefficients, whereas \mathcal{C} coefficients apply to the DLEFT coefficients.

Furthermore, Λ and Λ_L refer to the cutoff scale of respectively DSMEFT and DLEFT. These cutoff scales need not be identical, thus we distinguish them here. In the last line we introduce μ_M , the matching scale, the energy scale at which we match both theories. The matching of the Wilson coefficients occurs at the specified matching scale. In this case, we choose μ_M such that $\mu_M = \mu_R$. Recall that we mentioned that μ_R should be close to the weak scale in section 2.4. We can choose μ_R arbitrarily, but by demanding $\mu_R = \mu_M$ when matching DLEFT to DSMEFT, we only need to introduce one chosen energy scale. But, while μ_R can be chosen arbitrarily, μ_M is determined by the energy scale where one performs the matching. We know that the predictions of DLEFT break down above the cutoff energy Λ_L , which is near the weak scale. For our purposes, we can thus set $\mu_R = \Lambda_L$. A logical energy scale would be $\Lambda_L = m_W$, as all particles with a higher mass are integrated out of DLEFT. Summarising, we demand that $\mu_R = \mu_M$, and we identify that m_{μ_M} is constrained by the energy scale where we perform the matching, which is close to the electroweak scale in our case.

2.6.2 Matching at one-loop Level

We now expand the tree level matching by including the one-loop amplitudes:

$$\frac{2\mathcal{C}_{e\phi^2}}{\Lambda_L} = \mathcal{A}_{LO}(\mu_M) + \mathcal{A}_{NLO}(\mu_M) \quad (2.84)$$

Combining the above with (2.73, 2.80) gives us the relation between the DLEFT Wilson coefficient $\mathcal{C}_{e\phi^2}$ and the DSMEFT coefficients at one-loop level.

$$\begin{aligned} \mathcal{C}_{e\phi^2}(\mu_M) = & \frac{\Lambda_L m_e}{\Lambda^2} \left[C_{e\phi^2} - \frac{4C_{H^4\phi^2}(\mu_M)m_W^2 \sin(\theta_W)^2}{e^2 m_H^2} + \right. \\ & \frac{e^2}{64\pi^2 m_H^2 m_Z^2} \left\{ \frac{6(2 \log\left(\frac{\mu_M^2}{m_H^2}\right) + 1)C_{(DH)^2\phi^2} m_H^4}{\sin(2\theta_W)^2} \right. \\ & + m_Z^4 \left(- \frac{3(4 \log\left(\frac{\mu_M^2}{m_W^2}\right) + 2 \log\left(\frac{\mu_M^2}{m_Z^2}\right) - 1)(C_{(DH)^2\phi^2} + 4C_{W\phi^2})}{\sin(\theta_W)^2} \right. \\ & + 2(6 \log\left(\frac{\mu_M^2}{m_W^2}\right) - 1)(C_{(DH)^2\phi^2} + 4C_{W\phi^2}) - \frac{(6 \log\left(\frac{\mu_M^2}{m_Z^2}\right) - 1)(4C_{B\phi^2} + C_{(DH)^2\phi^2})}{\cos(\theta_W)^2} \\ & + m_H^2 m_Z^2 \left(\frac{\cos(2\theta_W)(4(6 \log\left(\frac{\mu_M^2}{m_Z^2}\right) - 1)C_{B\phi^2} - 6C_{(DH)^2\phi^2}) - 3C_{B\phi^2}}{\cos(\theta_W)^2} \right. \\ & \left. \left. \left. - 4(6 \log\left(\frac{\mu_M^2}{m_Z^2}\right) - 1)(C_{B\phi^2} - C_{W\phi^2}) \cos(2\theta_W) - \frac{9C_{W\phi^2}}{\sin(\theta_W)^2} \right) \right\} \right] \quad (2.85) \end{aligned}$$

Note that all DSMEFT Wilson coefficients on the right hand side of (2.85) are defined at the matching scale μ_M . For readability we write $C(\mu_M) \equiv C$ for all DSMEFT Wilson coefficients in

(2.85). Additionally, the matching scale sets the value for μ_R such that $\mu_R \equiv \mu_M$, where we follow the same argumentation that was given in the previous section. In this final definition, we note that $C_{W\phi^2}, C_{B\phi^2}$ and $C_{(DH)^2\phi^2}$ are the Wilson coefficients that arise firstly at one-loop level. In the previous section we have seen that the leading order coefficient for $C_{H^4\phi^2}$ is already given by the tree-level matching. As our aim is to only provide NLO corrections for Wilson coefficients that do not appear at tree level, our final definition of the matching does not include the terms proportional to $C_{H^4\phi^2}$ that arise in our one-loop calculations. The corrections to $C_{H^4\phi^2}$ are also incomplete, as one needs to include many more diagrams, including SM corrections, to obtain the complete set of NLO corrections to the tree level contribution of $C_{H^4\phi^2}$. Thus, the leading order matching contributions for all Wilson coefficients other than $C_{e\phi^2}$ and $C_{H^4\phi^2}$ are given by the one-loop matching and the NLO corrections for $C_{H^4\phi^2}$ are discarded in this definition.

Conclusion and Discussion

The goal of this research was to provide a one-loop matching between two effective field theories that include a Dark Matter scalar ϕ , where we focused on DM-electron scattering. We have seen that the usage of EFTs in DM research has proliferated over the years, but the matching of DM EFTs to one another generally remains limited to tree level. We aim to append to this line of research, by providing a matching procedure at one-loop level. In this thesis, we have given a complete set of NLO corrections to the tree level matching of the proposed DMSEFT and DLEFT for the Wilson coefficients $C_{W\phi^2}, C_{B\phi^2}, C_{(DH)^2\phi^2}$. These coefficients do not contribute at tree level, and as such they can be seen as a truly novel addition to the matching procedure. The full results for our matching are given by (2.85). By including these NLO effects in the matching procedure, we open the possibility to research a new portal between the DM and SM sector. This is especially relevant as the Higgs portal model has become more and more constrained.

The results of the matching procedure as presented in this research show that contributions from Wilson coefficients that do not occur at tree level may indeed arise when one includes NLO effects in their matching procedure. One-loop matching procedures may thus provide a promising avenue in Dark Matter research.

To properly cater to a more realistic experimental context, some additional steps need to be taken. Firstly, we have taken the decision to perform the matching for on-shell electrons. Note that at tree level, the on and off-shell amplitudes are identical. It is only at one-loop level that the difference between on and off-shell electrons comes into play, so when working at next to leading order, it becomes relevant to study off-shell effects. One needs to take off-shell effects into account, as one cannot make the on-shell assumption for bound electrons in direct detection experiments. Although we have identified that the results of only two one-loop amplitudes are changed by setting the electrons on-shell, we do as of yet not know what effect setting the electrons on-shell would have on experimental predictions.

Secondly, we have linked DSMEFT, a theory that is valid at SM energies, to DLEFT, a theory that is valid below the electroweak scale. Direct detection experiments work at even lower energies, so a second matching procedure linking DLEFT to a non-relativistic EFT is needed to make proper experimental predictions. Thirdly, we have not studied the contributions of photonic effects at one-loop order. Such effects may be suppressed, but a more comprehensive study is needed to make more certain statements. Finally, our proposed DSMEFT only introduces a DM scalar. Further research could repeat the steps taken for vector or fermion DM, for example.

Bibliography

- [1] Katherine Garrett and Gintaras Duda. “Dark matter: A primer”. In: *Advances in Astronomy* 2011 (2011), pp. 1–22.
- [2] Jason Aebischer et al. “Dark matter effective field theory and an application to vector dark matter”. In: *Journal of High Energy Physics* 2022.6 (2022), pp. 1–39.
- [3] Francesco D’Eramo and Massimiliano Procura. “Connecting dark matter UV complete models to direct detection rates via effective field theory”. In: *Journal of High Energy Physics* 2015.4 (2015), pp. 1–40.
- [4] Varun Sahni. “Dark matter and dark energy”. In: *arXiv preprint astro-ph/0403324* (2004).
- [5] Leszek Roszkowski, Enrico Maria Sessolo, and Sebastian Trojanowski. “WIMP dark matter candidates and searches—current status and future prospects”. In: *Reports on Progress in Physics* 81.6 (2018), p. 066201.
- [6] Julien Billard et al. “Direct detection of dark matter—APPEC committee report*”. In: *Reports on Progress in Physics* 85.5 (Apr. 2022), p. 056201. DOI: [10.1088/1361-6633/ac5754](https://doi.org/10.1088/1361-6633/ac5754). URL: <https://dx.doi.org/10.1088/1361-6633/ac5754>.
- [7] Benjamin Audren et al. “Strongest model-independent bound on the lifetime of Dark Matter”. In: *Journal of Cosmology and Astroparticle Physics* 2014.12 (Dec. 2014), pp. 028–028. DOI: [10.1088/1475-7516/2014/12/028](https://doi.org/10.1088/1475-7516/2014/12/028). URL: <https://doi.org/10.1088/1475-7516/2014/12/028>.
- [8] Gianfranco Bertone and Dan Hooper. “History of dark matter”. In: *Reviews of Modern Physics* 90.4 (2018), p. 045002.
- [9] Gianfranco Bertone, Dan Hooper, and Joseph Silk. “Particle dark matter: Evidence, candidates and constraints”. In: *Physics reports* 405.5-6 (2005), pp. 279–390.
- [10] Lars Bergström. “Dark matter candidates”. In: *New Journal of Physics* 11.10 (2009), p. 105006.

- [11] Leszek Roszkowski, Enrico Maria Sessolo, and Sebastian Trojanowski. “WIMP dark matter candidates and searches—current status and future prospects”. In: *Reports on Progress in Physics* 81.6 (May 2018), p. 066201. DOI: [10.1088/1361-6633/aab913](https://doi.org/10.1088/1361-6633/aab913). URL: <https://doi.org/10.1088/1361-6633/aab913>.
- [12] Giorgio Arcadi et al. “The waning of the WIMP? A review of models, searches, and constraints”. In: *The European Physical Journal C* 78 (2018), pp. 1–57.
- [13] E Aprile et al. “First Dark Matter Search with Nuclear Recoils from the XENONnT Experiment”. In: *arXiv preprint arXiv:2303.14729* (2023).
- [14] Marc Schumann. “Direct detection of WIMP dark matter: concepts and status”. In: *Journal of Physics G: Nuclear and Particle Physics* 46.10 (Aug. 2019), p. 103003. DOI: [10.1088/1361-6471/ab2ea5](https://dx.doi.org/10.1088/1361-6471/ab2ea5). URL: <https://dx.doi.org/10.1088/1361-6471/ab2ea5>.
- [15] Teresa Marrodán Undagoitia and Ludwig Rauch. “Dark matter direct-detection experiments”. In: *Journal of Physics G: Nuclear and Particle Physics* 43.1 (Dec. 2015), p. 013001. DOI: [10.1088/0954-3899/43/1/013001](https://dx.doi.org/10.1088/0954-3899/43/1/013001). URL: <https://dx.doi.org/10.1088/0954-3899/43/1/013001>.
- [16] Tongyan Lin. “Sub-GeV dark matter models and direct detection”. In: *SciPost Physics Lecture Notes* (2022), p. 043.
- [17] Riccardo Catena et al. “Dark matter-electron interactions in materials beyond the dark photon model”. In: *Journal of Cosmology and Astroparticle Physics* 2023.03 (2023), p. 052.
- [18] Pietro Di Gangi. “The Xenon Road to Direct Detection of Dark Matter at LNGS: The XENON Project”. In: *Universe* 7.8 (2021), p. 313.
- [19] Aneesh V Manohar. “Introduction to effective field theories”. In: (2018).
- [20] David B Kaplan. “Five lectures on effective field theory”. In: *arXiv preprint nucl-th/0510023* (2005).
- [21] Matthias Neubert. “Effective field theory and heavy quark physics”. In: *Physics In D 4 Tasi 2004: TASI 2004*. World Scientific, 2006, pp. 149–194.
- [22] A Liam Fitzpatrick et al. “The effective field theory of dark matter direct detection”. In: *Journal of Cosmology and Astroparticle Physics* 2013.02 (2013), p. 004.
- [23] Joachim Brod et al. “Effective field theory for dark matter direct detection up to dimension seven”. In: *Journal of High Energy Physics* 2018.10 (2018), pp. 1–28.
- [24] E Aprile et al. “Effective Field Theory and Inelastic Dark Matter Results from XENON1T”. In: *arXiv preprint arXiv:2210.07591* (2022).

- [25] Giorgio Arcadi, Abdelhak Djouadi, and Martti Raidal. “Dark Matter through the Higgs portal”. In: *Physics Reports* 842 (2020). Dark Matter through the Higgs portal, pp. 1–180. ISSN: 0370-1573. DOI: <https://doi.org/10.1016/j.physrep.2019.11.003>. URL: <https://www.sciencedirect.com/science/article/pii/S0370157319304004>.
- [26] Giampiero Passarino and M.J.G. Veltman. “One-loop corrections for e^+e^- annihilation into $\mu^+\mu^-$ in the Weinberg model”. In: *Nuclear Physics B* 160.1 (1979), pp. 151–207.
- [27] M. Veltman et al. “Scalar one-loop integrals”. In: *Nuclear Physics B* 153 (1979), pp. 365–401.
- [28] Ansgar Denner and Stefan Dittmaier. “Reduction schemes for one-loop tensor integrals”. In: *Nuclear Physics B* 734.1-2 (2006), pp. 62–115.
- [29] Ansgar Denner. “Techniques for the Calculation of Electroweak Radiative Corrections at the One-Loop Level and Results for W-physics at LEP 200”. In: *Fortschritte der Physik/Progress of Physics* 41.4 (1993), pp. 307–420.
- [30] Vladyslav Shtabovenko, Rolf Mertig, and Frederik Orellana. “FeynCalc 9.3: New features and improvements”. In: *Computer Physics Communications* 256 (Nov. 2020), p. 107478. DOI: [10.1016/j.cpc.2020.107478](https://doi.org/10.1016/j.cpc.2020.107478). URL: <https://doi.org/10.1016%5C%2Fj.cpc.2020.107478>.
- [31] Hiren H. Patel. “Package-X: A Mathematica package for the analytic calculation of one-loop integrals”. In: *Computer Physics Communications* 197 (2015), pp. 276–290.
- [32] Vladyslav Shtabovenko. “FeynHelpers: Connecting FeynCalc to FIRE and Package-X”. In: *Computer Physics Communications* 218 (Sept. 2017), pp. 48–65. DOI: [10.1016/j.cpc.2017.04.014](https://doi.org/10.1016/j.cpc.2017.04.014). URL: <https://doi.org/10.1016%5C%2Fj.cpc.2017.04.014>.
- [33] Adam Alloul et al. “FeynRules 2.0 — A complete toolbox for tree-level phenomenology”. In: *Computer Physics Communications* 185.8 (Aug. 2014), pp. 2250–2300. DOI: [10.1016/j.cpc.2014.04.012](https://doi.org/10.1016/j.cpc.2014.04.012). URL: <https://doi.org/10.1016%2Fj.cpc.2014.04.012>.
- [34] Thomas Hahn. “Generating Feynman diagrams and amplitudes with FeynArts 3”. In: *Computer Physics Communications* 140.3 (2001), pp. 418–431. ISSN: 0010-4655. DOI: [https://doi.org/10.1016/S0010-4655\(01\)00290-9](https://doi.org/10.1016/S0010-4655(01)00290-9). URL: <https://www.sciencedirect.com/science/article/pii/S0010465501002909>.
- [35] Katelin Schutz and Kathryn M. Zurek. “Detectability of light dark matter with superfluid helium”. In: *Physical review letters* 117.12 (2016), p. 121302.
- [36] Andrzej J. Buras. “Weak Hamiltonian, CP violation and rare decays”. In: *arXiv preprint hep-ph/9806471* (1998).
- [37] Matthias Neubert. “Renormalization theory and effective field theories”. In: *Effective Field Theory in Particle Physics and Cosmology: Lecture Notes of the Les Houches Summer School: Volume 108, July 2017* 108 (2020), p. 1.